Novel bicistronic lentiviral vectors correct β-Hexosaminidase deficiency in neural and hematopoietic stem cells and progeny: implications for *in vivo* and *ex vivo* gene therapy of GM2 gangliosidosis

Francesca Ornaghi[a], Davide Sala[a,b], Fabiana Tedeschi[a], Maria Chiara Maffia[a], Martina Bazzucchi[b], Francesco Morena[b], Manuela Valsecchi[c], Massimo Aureli[c], Sabata Martino[b], Angela Gritti[a,*]

[a] *San Raffaele Telethon Institute for Gene Therapy (SR-Tiget), IRCCS San Raffaele Scientific Institute, Via Olgettina 60, 20132 Milan, Italy*
[b] *Department of Chemistry, Biology and Biotechnology, University of Perugia, Via del Giochetto, 06123 Perugia, Italy*
[c] *Department of Medical Biotechnology and Translational Medicine, University of Milano, Via Fratelli Cervi 93, 20090 Segrate, MI, Italy*

ABSTRACT

The favorable outcome of *in vivo* and *ex vivo* gene therapy approaches in several Lysosomal Storage Diseases suggests that these treatment strategies might equally benefit GM2 gangliosidosis. Tay-Sachs and Sandhoff disease (the main forms of GM2 gangliosidosis) result from mutations in either the *HEXA* or *HEXB* genes encoding, respectively, the α- or β-subunits of the lysosomal β-Hexosaminidase enzyme. In physiological conditions, α- and β-subunits combine to generate β-Hexosaminidase A (HexA, αβ) and β-Hexosaminidase B (HexB, ββ). A major impairment to establishing *in vivo* or *ex vivo* gene therapy for GM2 gangliosidosis is the need to synthesize the α- and β-subunits at high levels and with the correct stoichiometric ratio, and to safely deliver the therapeutic products to all affected tissues/organs.

Here, we report the generation and *in vitro* validation of novel bicistronic lentiviral vectors (LVs) encoding for both the murine and human codon optimized *Hexa* and *Hexb* genes. We show that these LVs drive the safe and coordinate expression of the α- and β-subunits, leading to supranormal levels of β-Hexosaminidase activity with prevalent formation of a functional HexA in SD murine neurons and glia, murine bone marrow-derived hematopoietic stem/progenitor cells (HSPCs), and human SD fibroblasts. The restoration/overexpression of β-Hexosaminidase leads to the reduction of intracellular GM2 ganglioside storage in transduced and in cross-corrected SD murine neural progeny, indicating that the transgenic enzyme is secreted and functional. Importantly, bicistronic LVs safely and efficiently transduce human neurons/glia and CD34+ HSPCs, which are target and effector cells, respectively, in prospective *in vivo* and *ex vivo* GT approaches.

We anticipate that these bicistronic LVs may overcome the current requirement of two vectors co-delivering the α- or β-subunits genes. Careful assessment of the safety and therapeutic potential of these bicistronic LVs in the SD murine model will pave the way to the clinical development of LV-based gene therapy for GM2 gangliosidosis.

1. Introduction

Sandhoff disease (SD) and Tay-Sachs disease (TSD) (the main forms of GM2 gangliosidosis) are rare neurodegenerative lysosomal storage disease (LSD) caused by mutations in the *HEXB* and *HEXA* genes, respectively, encoding for the β- and α-subunit of the β-Hexosaminidase enzyme (E.C.3.2.1.52; β-Hex) (Sandhoff and Harzer, 2013). HexA, an αβ heterodimer, and HexB, a ββ homodimer, are the two major forms of β-Hex (Gravel et al., 1991), while HexS (αα) is a minor form with

negligible catalytic activity (Ellis et al., 1975; Ikonne et al., 1975). The lysosomal accumulation of GM2 ganglioside and related glycolipids consequent to β-Hex deficiency is ubiquitous but particularly abundant in CNS tissues and neurons, which undergo severe and progressive dysfunction and death (Huang et al., 1997; Phaneuf et al., 1996; Sango et al., 2002). In the most severe (infantile) forms of SD and TSD clinical decline is rapid and death occurs a few years after the diagnosis (Regier et al., 2016).

There are currently no treatments for GM2 gangliosidosis. The

A

LV.mA [hPGK] [mHexa] [WPRE]

LV.mB [hPGK] [mHexb] [WPRE]

LV.mAB [hPGK] [mHexb^C.O.] [P2A] [mHexa^C.O.] [WPRE]

LV.hAB [hPGK] [hHexb^C.O.] [P2A] [hHexa^C.O.] [WPRE]
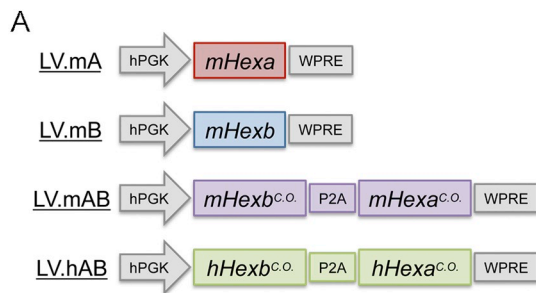
B

Vector	MOI	Vector Copy Number (mean ± SEM)
LV.mB	50	2,40 ± 0,24
LV.mA + LV.mB	50 + 50	3,85 ± 1,46
LV.mAB	50	5,82 ± 2,88
LV.hAB	50	3,68 ± 2,33

C

D

E

F
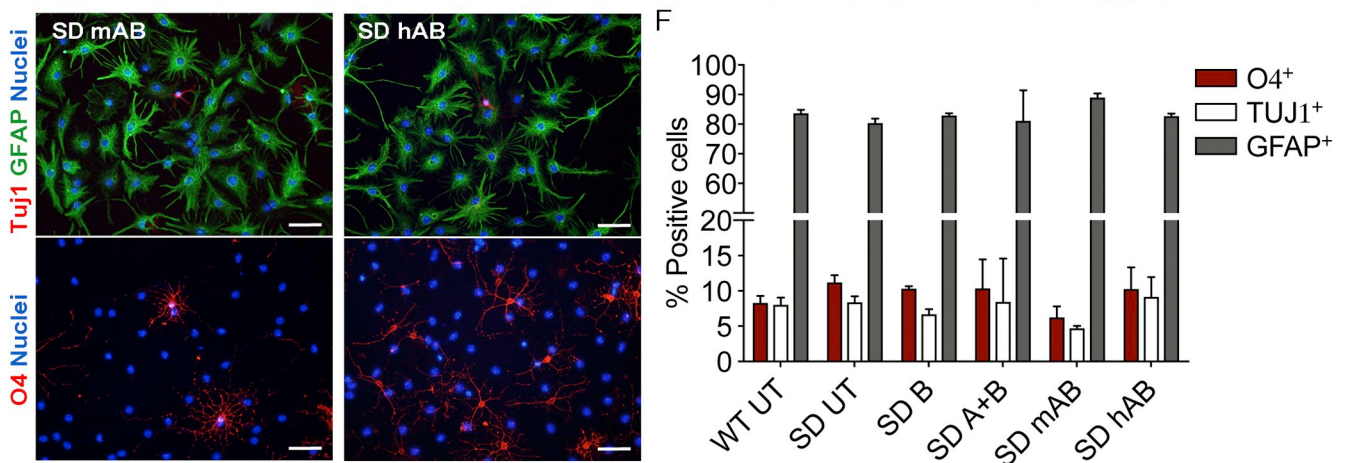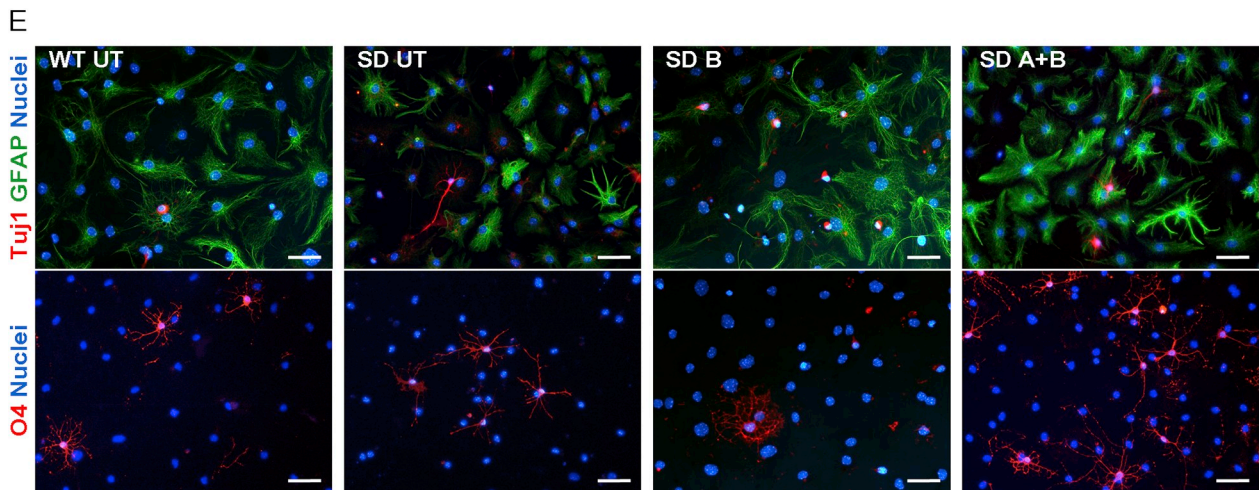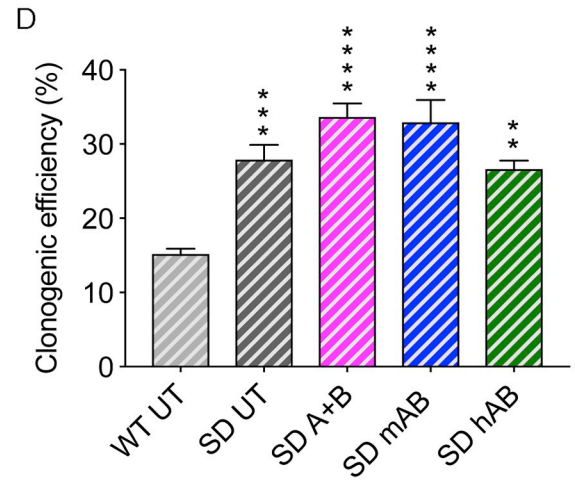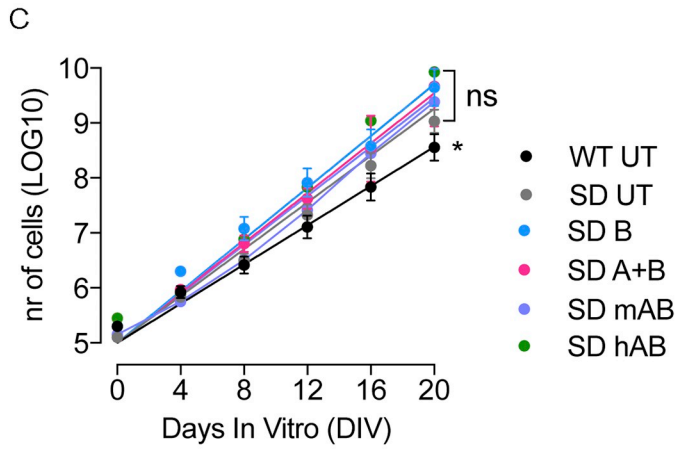
(caption on next page)

Fig. 1. Functional characterization of LV-transduced NPCs.
(A) Schematic of mono- and bicistronic lentiviral vectors. (B) VCN values of SD NPCs transduced with the different LVs at MOI 50 or MOI 50 + 50 for the co-delivered LVs. Values are the mean ± SEM; $n = 3$ independent experiments, 5–6 replicates/group. (C) Population analysis showing long-term proliferation and stable expansion rate of WT and SD NPC lines (subculturing passages 0 to 5 shown in the graph; up to 20 days *in vitro*, DIV). Each point of the curves represents the mean ± SEM; $n = 2$–3 independent experiments, 2 NPC lines. Data were interpolated using a linear regression model and best fitted the following equation: $y = a + bx$, where y is the estimated total number of cells (in log scale), x is the time (days *in vitro*, DIV), *a* is the intercept, and *b* is the slope. Slope values (b) $+/-$ SEM are the following: WT UT, 0.178 ± 0.006; SD UT, 0.213 ± 0.005; SD B, 0.235 ± 0.008; SD A + B, 0.227 ± 0.01; SD mAB, 0.223 ± 0.005; SD hAB, 0.235 ± 0.007. Data analysed by One-way Anova followed by Dunnet's multiple comparison test. $*p < .05$ *vs* all SD lines. ns, not significant *vs* SD UT line. (D) Clonogenic efficiency of WT and SD NPCs (UT and LV-transduced). Data are the mean ± SEM; n = 3 independent experiments, in duplicate. Data analysed by One-Way Anova followed by Dunnet's multiple comparison test, $** p < .001$, $*** p < .0005$, $**** p < .0001$ *vs* WT UT. (E) Representative pictures of WT and SD differentiated progeny after immunofluorescence analysis using anti-Tuj1 (red), anti-GFAP (green) and anti-O4 (red) antibodies to stain neurons, astrocytes and oligodendrocytes, respectively. Nuclei are counterstained with Hoechst (blue). Magnification: 20×. Scale bar, 50 μm. (F) Cell type composition of WT and SD (UT and LV-transduced) differentiated cultures. Data are expressed as percentage of immunoreactive (IR) cells on total nuclei and represent the mean ± SEM of $n = 4$ experiments, 2 coverslips/group.

infusion of the recombinant enzyme (von Specht et al., 1979; Tsuji et al., 2011; Matsuoka et al., 2011), pharmacological chaperones (Maegawa et al., 2007), or drugs inhibiting the synthesis of glycosphingolipids (Andersson et al., 2004) are ineffective in infantile patients and provide only partial benefit in late-onset forms (von Specht et al., 1979; Maegawa et al., 2009; Clarke et al., 2011; Tallaksen and Berg, 2009). Transplantation of hematopoietic stem/progenitor cells (HSPCs) ameliorates neuroinflammation and prolongs the lifespan of Sandhoff mice ($Hexb^{-/-}$; resembling symptoms and progression of the infantile disease forms) (Sango et al., 1996) but fails to counteract GM2 storage in CNS tissues, likely because of insufficient levels of β-Hex delivered by the HSPC-derived myeloid progeny (Norflus et al., 1998; Wada et al., 2000). In line with these observations, allogeneic hematopoietic stem cell (HSC) transplant provides minimal benefit to SD and TSD patients (Hoogerbrugge et al., 1995). An autologous HSC gene therapy (GT) approach could overcome the limitation of allogeneic HSCT; in fact, decreasing transplant-related side effects could enhance the therapeutic advantage expected from vector-mediated enzyme supra-physiological expression in HSPCs and their myeloid progeny that repopulate the CNS, PNS, and periphery. The remarkable benefit observed in infantile metachromatic leukodystrophy patients (MLD; a fatal neurodegenerative LSD) upon transplantation of autologous HSPCs engineered using lentiviral vectors (LV) to overexpress ARSA (the enzyme missing in MLD) (Biffi et al., 2013; Sessa et al., 2016) provides a strong rationale for translating this approch to GM2 gangliosidos. However, whether HSPCs can safely produce and secrete therapeutically relevant quantities of functional HexA (the only isoform able to degrade GM2 ganglioside) (Gravel et al., 1991) by LV-mediated genetic manipulation is currently not known.

In vivo intracerebral (IC) GT with adeno-associated virus (AAV)-mediated β-Hex expression ameliorates the pathology of SD mice (Cachon-Gonzalez et al., 2014; Osmon et al., 2016) and cats (McCurdy et al., 2015; Rockwell et al., 2015). So far, the co-delivering of two AAVs expressing the α- and β-subunits is required to generate therapeutic amounts of functional HexA (Cachon-Gonzalez et al., 2014; Bradbury et al., 2013; Gray-Edwards et al., 2017), adding difficulties to the prospective clinical exploitation of this treatment approach. Novel AAVs driving the expression of both subunits (Woodley et al., 2019) or of a hybrid subunit (Tropak et al., 2016) may address this issue. However, the immunogenicity of AAVs (Mingozzi and High, 2013), the potential immune response triggered by a chimeric transgene, and the toxicity associated to AAV-mediated β-Hex overexpression in CNS tissues (Golebiowski et al., 2017) demand long-term efficacy and safety assessment in relevant animal models in view of the clinical translation of this approach.

The negligible immunogenicity and safe integration profile in neural tissues (Bartholomae et al., 2011; Lattanzi et al., 2014; Meneghini et al., 2016) make LVs effective vehicles in the context of IC GT approaches for LSDs. Importantly, the large LV packaging size allows the simultaneous expression of multiple genes in multicistronic constructs (Palfi et al., 2014). Earlier studies have proposed bicistronic LVs to

achieve metabolic correction in SD human fibroblasts and murine neurons (Arfi et al., 2005; Arfi et al., 2006). However, a comprehensive investigation of the efficacy and safety of these vectors in relevant murine and human cell types is lacking.

In this work, we report the generation and *in vitro* validation of novel bicistronic LVs driving the safe expression of the α- and β-subunits of the β-Hex enzyme, leading to supranormal levels of β-Hex activity and favoring the formation of a functional HexA in SD murine neurons and glia, bone marrow-derived murine HSPCs, and human SD fibroblasts. The restoration/overexpression of β-Hex leads to the reduction of intracellular GM2 ganglioside storage in transduced and in cross-corrected SD murine neural progeny, demonstrating that the transgenic enzyme is secreted and functional. Importantly, bicistronic LVs safely and efficiently transduce human neurons/glia and CD34 + HSPCs, which model target and effector cells, respectively, in prospective *in vivo* and *ex vivo* GT approaches to treat GM2 gangliosidosis.

2. Results

2.1. Design and production of mono- and bicistronic lentiviral vectors carrying the Hexa and Hexb genes

We designed and produced four third-generation VSV-G-pseudo-typed lentiviral vectors (LVs) encoding the murine (m) *Hexa* and *Hexb,* and the human (h) *HEXA* and *HEB* genes under the control of the ubiquitous human phosphoglycerate kinase (PGK) promoter. In the bicistronic LVs, the codon-optimized genes were linked by a 2A peptide (P2A) sequence. The different vectors were called LV.mA, LV.mB, LV.mAB, and LV.hAB, encoding the murine β-Hex α-chain, β-chain, and both the α- and β-chains (murine and human), respectively (Fig. 1A). Titer and infectivity of the LV batches were in the range of 0.6–2.7*10^9 TU/ml and 3–7*10^4 TU/ng, respectively (see Materials and Methods).

2.2. Efficient and safe transduction of SD neural stem/progenitor cells by mono- and bicistronic LVs

We used neural stem/progenitor cells (NPCs) derived from SD mice as a relevant *in vitro* model to test the efficacy and safety of the mono- and bicistronic LVs. The rationale is based on our previous results showing that patterns of β-Hex activity, isoenzyme composition, gene expression, and ganglioside metabolism observed during embryonic and postnatal brain development of TSD and SD mice ($Hexb^{-/-}$) are recapitulated during the stages of TSD and SD NPC differentiation to mature glia and neurons *in vitro* (Martino et al., 2009).

SD NPCs were transduced with the different LVs at 50 multiplicity of infection (MOI 50) according to optimized protocols (Neri et al., 2011). Untransduced (UT) SD and WT cells were used as controls. All LVs proficiently transduced murine NPCs, as shown by the presence of integrated LV genome copies in each condition tested (vector copy number, VCN; range 2–6) (Fig. 1B). Importantly, LV transduction did not affect the cardinal NPC functional properties, namely proliferation,

self-renewal, and multipotency. LV-transduced and UT NPCs showed long-term proliferation when serially subcultured in the presence of FGF2 and EGF (Gritti et al., 2009). The trend for a higher proliferation rate observed in SD NPCs (both UT and LV-transduced) (Fig. 1C) may reflect a higher content of stem/progenitor cells in the SD as compared to the WT cell populations, as also suggested by the increased clonogenic efficiency (Fig. 1D). This feature did not affect NPC multipotentiality. Indeed, immunofluorescence (IF) analysis using antibodies against lineage-specific markers followed by quantification of cells immunoreactive for the different antigens showed similar proportions of neurons (TUJ1), astrocytes (GFAP), and oligodendrocytes (O4) in both UT and LV-transduced NPC-derived progeny (*differentiated cells*, obtained by culturing NPCs in FGF2 for 2 days and then in a mitogen-free medium supplemented with 2% FBS for additional 5 days) (Fig. 1E–F).

Overall these data show that transduction using mono- and bicistronic LVs is well tolerated by NPCs and does not impact on their functional features.

2.3. Stable expression of the α- and β-subunits, supranormal β-Hex activity, and correct isoenzyme composition mediated by bicistronic LVs in SD NPCs and progeny

We assessed the efficacy of bicistronic LVs in achieving optimal expression of the α- and β-subunit, correct isoenzyme composition, and restoration of β-Hex activity. To this end, we measured the mRNA expression of murine and human Hex genes, β-Hex activity and isoforms in two NPC-derived types of cultures (UT and LV-transduced): i) a cell population enriched in proliferating and undifferentiated cells, obtained by culturing NPCs for two days in EGF + FGF2 (*precursor cells*); (ii) NPC-derived mixed neuronal/glial cultures (*differentiated cells;* see Fig. 1E–F).

We assessed mRNA expression by qPCR exploiting probes recognizing the native or the codon-optimized sequences of the Hex genes. The probes toward the native sequence allowed us determining: i) the endogenous (physiological) *Hexa* and *Hexb* mRNA in untreated (UT) WT and SD cells; ii) the total level of Hexa and Hexb mRNA (endogenous + transgenic) in NPCs transduced with monocistronic vectors, whose sequence is not codon-optimized (LV.mA, LV.mB); iii) the endogenous mRNA in NPCs transduced with bicistronic vectors (LV.mAB, LV.hAB). The probes toward the codon-optimized sequences do not recognize the native sequences, thus detecting only the transgenic mRNA in cells transduced with bicistronic vectors.
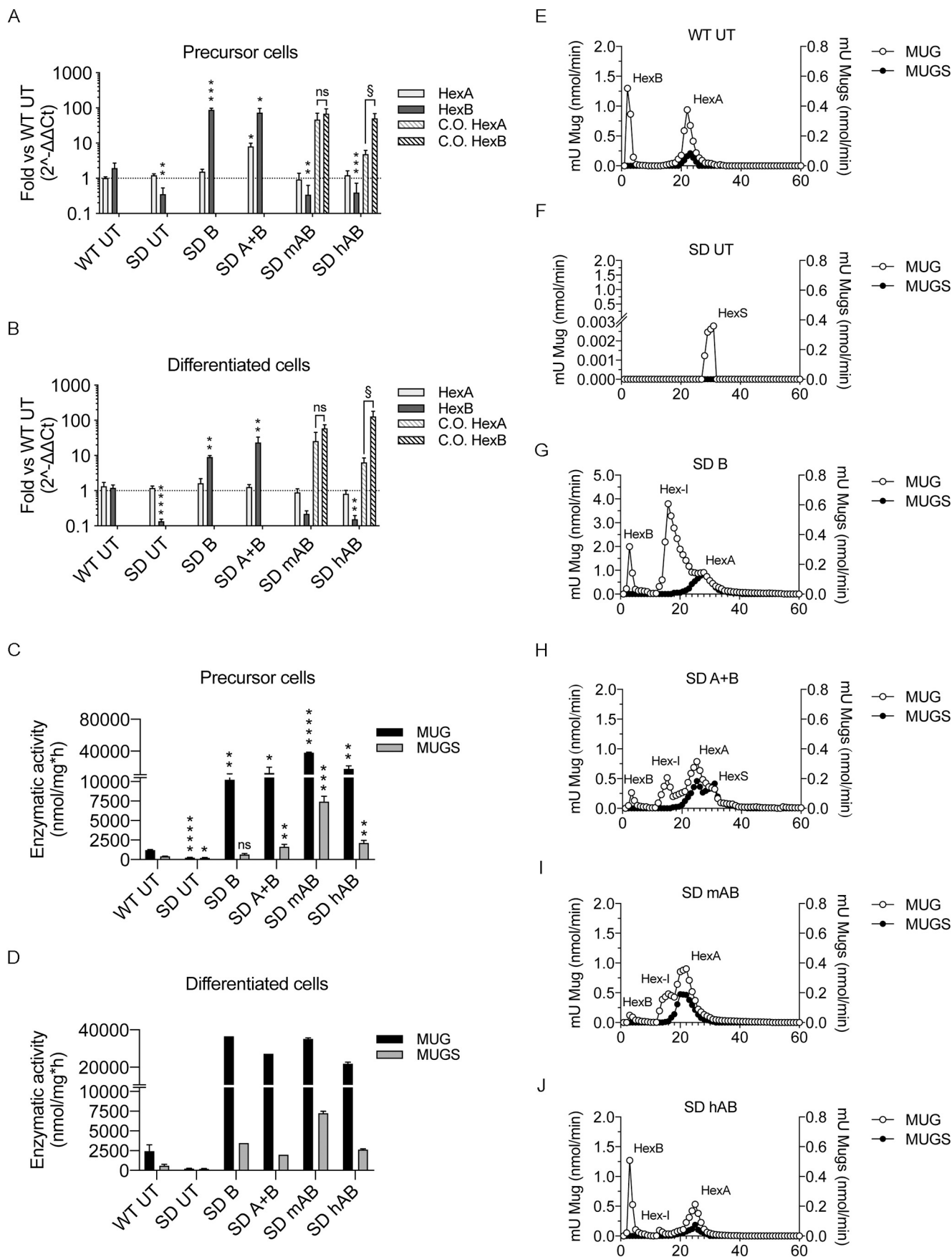
UT SD precursors (Fig. 2A) and differentiated cells (Fig. 2B) showed normal pattern of endogenous *Hexa* and strongly reduced levels of endogenous *Hexb* mRNA expression as compared to the WT counterpart. LV.mB-transduced SD cells displayed a significant upregulation of total *Hexb* mRNA expression ($\approx$100- and $\approx$20-fold the WT levels in precursors and differentiated cells, respectively, mainly reflecting the transgene overexpression given the low endogenous levels), without changes in the endogenous *Hexa* mRNA expression. The co-delivery of monocistronic LVs (LV.mA + LV.mB) in SD cells resulted in upregulation of both genes, with a 10-fold higher expression of total *Hexb* as compared to total *Hexa* mRNA expression (Fig. 2A–B). The expression of transgenic *Hexb* and *Hexa* mRNAs (codon optimized sequence) was high and comparable in SD cells transduced with the bicistronic LV.mAB (up to 30-fold the normal levels), while a 10-fold higher expression of the codon-optimized *HEXB* as compared to *HEXA* was detected in LV.hAB-transduced murine SD cells (Fig. 2A–B). Neither in precursor nor in differentiated cells the upregulation of the murine and human codon optimized transgenes did affect the expression level of the endogenous *Hexa* and *Hexb* genes (Fig. 2A–B).

The advantage of bicistronic LVs as compared to the co-delivery of monocistronic LVs in achieving stoichiometric expression of *Hexa* and *Hexb* genes was further confirmed by assessing β-Hex enzymatic activity in transduced cells using two artificial substrates: MUG is

hydrolysed by both α and β subunits, and therefore by HexA (αβ), HexB (ββ), and HexS (αα); MUGS is hydrolysed only by the α subunit, and therefore by HexA and HexS. UT SD cells show barely detectable levels of MUG- and MUGS-related enzymatic activity (Fig. 2C, precursors; Fig. 2D, differentiated cells). Transduction of SD cells with LV.mB was sufficient to achieve supraphysiological level of enzymatic activity (8- and 5-fold the WT levels for precursors and differentiated cells with MUG, respectively) (Fig. 2C-D). Transduction with LV.mB + LV.mA and bicistronic LVs ensured supraphysiological enzymatic activity ($\approx$10–40-fold the WT levels). Of note, we detected +30% and +100% of MUG and MUGS-related activity, respectively, in SD cells transduced with bicistronic LVs as compared to those transduced with LV.mA + LV.mB, resulting in close to physiological MUG/MUGS ratio ($\approx$2 and $\approx$4 in WT precursors and differentiated cells, respectively) (Fig. 2C–D). Importantly, the supraphysiological enzymatic activity was achieved using half the vector dose with bicistronic LVs. The pattern of enzymatic reconstitution upon transduction with different LVs was stable along NPC differentiation toward neurons and glia (Suppl. Fig. 1A–B).

The chromatographic analysis corroborated the evidence of LV-mediated β-Hex rescue/overexpression and, in combination with the enzymatic assay through MUG and MUGS substrates, provided additional information about the subunit composition of Hex isoenzymes (Martino et al., 2009; Martino et al., 1997; Martino et al., 2005). In our experimental conditions HexB was eluted with the void volume from the column, whereas HexA, HexS, and intermediate forms were retained by the column and eluted with a linear gradient of NaCl (0.0–0.5 M) based on their respective isoelectric points. The chromatographic profile of WT UT NPCs (Fig. 2E) showed two peaks of activity corresponding to HexB (43% of total Hex activity) and HexA (57% of total Hex activity) (Suppl. Table 1). The isoenzyme ratio changed in differentiated cells, in which HexA accounted for $\approx$90% of total Hex activity (Suppl. Fig. 1C; Suppl. Table 1). In SD precursors (Fig. 2F) and differentiated cells (Suppl. Fig. 1D) the residual activity eluted with the high concentration of NaCl might correspond to HexS, due to the absence of the β-subunit. Transduction of SD NPCs with LV.mB caused the formation of HexB (11% of total Hex activity), HexA (36% of total Hex activity), and an additional consistent peak of activity (53% of total Hex activity) eluted at a lower NaCl concentration with respect to HexA and detectable only with the MUG substrate (Fig. 2G; Suppl. Table 1). This form might correspond to a Hex intermediate form composed of ββ precursors that we have documented in murine brain tissues during development and in NPCs and that we named HexI (Martino et al., 2009). In SD NPCs transduced with LV.mA + LV.mB the overexpression of both α and β subunits generated the formation of HexB (6% of total Hex activity), HexA (53% of total Hex activity), HexI (22% of total Hex activity), and HexS (9% of total Hex activity) (Fig. 2H; Suppl. Table 1). The transduction of SD NPCs with bicistronic LV.mAB generated a high amount of HexA (67% of total Hex activity) but little HexB (3% of total Hex activity) and a consistent HexI (30% of total Hex activity) suggesting that α and β subunits are still unbalanced (Fig. 2I; Suppl. Table 1). Finally, transduction of SD NPCs with bicistronic LV.hAB generated the formation of HexB (40% of total Hex activity), a small amount of HexI (6% of total Hex activity), and HexA (54% of total Hex activity) (Fig. 2J; Suppl. Table 1), as well as a chromatographic profile comparable to the WT UT counterpart. These isoenzyme patterns are maintained in differentiated cells (Suppl. Fig. 1E–F). Importantly, Western Blot analysis revealed that LV.hAB-transduced cells showed mature expression of the HexA and HexB proteins (Woodley et al., 2019; Tropak et al., 2016; Sinici et al., 2013; Utsumi et al., 2002) (Suppl. Fig. 1G).

Overall these data strongly suggest that bicistronic LVs drive a stoichiometric expression of α and β subunits that is not fully guaranteed by the co-delivery of monocistronic LVs and ensure a close to physiological reconstitution of isoenzyme composition coupled to supraphysiological levels of functional HexA and HexB.

(caption on next page)

Fig. 2. Gene expression, enzymatic activity and isoenzyme composition of LV-transduced NPCs.

(A–B) Expression of *Hexa* and *Hexb* mRNA in WT UT and SD (UT and LV-transduced) precursors (A) and differentiated cells (B). The mRNA expression was measured exploiting probes recognizing specifically the native (plain bars) *versus* the codon-optimized (C.O.) sequences (striped bars). In UT WT and SD cells the probes toward the native sequence detect the endogenous *Hexa* and *Hexb* mRNA; in NPCs transduced with monocistronic vectors (non C.O. sequence) the probes detect the total mRNA (endogenous + transgenic); in NPCs transduced with bicistronic vectors encoding C.O. sequences, we use the two types of probes to distinguish the endogenous (bearing the native sequence) *vs.* the transgenic (C.O.) mRNA. Values are the mean ± SEM and are expressed as fold *versus* the WT UT (set as 1). Gene expression is normalized on GAPDH. n = 3 independent experiments, 3 samples/group. Data were analysed by One-way ANOVA followed by Kruskal-Wallis multiple comparison test; * $p < .05$, ** $p < .01$, *** $p < .001$, **** $p < .0001$ *versus* WT UT; § $p < .05$ C.O. Hexb gene *vs.* C.O. Hexa gene.

(C–D) MUG- and MUGS- related enzymatic activity measured in WT UT and SD (UT and LV-transduced) precursors (C) and differentiated cells (D). Data were analysed by One-way ANOVA followed by Kruskal-Wallis multiple comparison test; * $p < .05$, ** $p < .01$, *** $p < .001$, **** $p < .0001$ *versus* WT UT.

(E–J) Diethylaminoethyl Cellulose (DEAE) chromatography showing the presence of HexA, HexB, HexS and HexI isoforms in WT and SD UT (E-F) and in LV-transduced SD precursors (G-J). Enzymatic activity (expressed as nmol/min; mU MUG on the left and mU MUGS on the right) and fraction number (0.5 ml) are plotted on the y and x axis, respectively.

2.4. Rescue of β-Hex activity and metabolic correction in LV-transduced and cross-corrected NPC-derived neurons and glial cells

Qualitative and quantitative IF analysis showed the expansion of the lysosomal compartment (LAMP1) and accumulation of GM2 ganglioside in SD NPC-derived progeny as compared to WT counterparts (Fig. 3A–C), with GM2-positive signal detected in both neurons and glial cells (Fig. 3D). Transduction with LV.mB only partially reduced GM2- and LAMP1-positive areas, which were instead normalized upon the delivery of both the α- and β-subunits, either by bicistronic LVs or co-delivery of the monocistronic LVs (Fig. 3A–C). These results confirm NPC cultures as a valuable model recapitulating the GM2 storage and lysosomal abnormalities that characterize SD pathology. In addition, they suggest that the functional HexA enzyme generated by the simultaneous delivery of α- and β-subunits is sufficient to rescue the primary biochemical and functional disease hallmarks in this *in vitro* culture system.

The therapeutic efficacy of gene therapy strategies greatly relies on the capability of genetically modified cells to secrete part of functional lysosomal enzyme for its uptake by neighbouring enzyme-deficient cells (metabolic cross-correction). In order to check the occurrence of cross-correction in our system, we exposed SD NPCs and progeny (*acceptor cells*) to the supernatant of WT UT or LV.mAB-transduced SD cells (*donor cells*) during the differentiation process (Suppl. Fig. 2A). At the end of the experiment, we analysed β-Hex activity and GM2 storage in SD cross-corrected neuronal/glial progeny. Supraphysiological enzymatic activity in LV.mAB-transduced SD NPCs (15-fold the normal) correlated to higher enzymatic activity in the supernatant (Fig. 4A–B and Suppl. Fig. 2B). The presence of supranormal *vs.* physiological levels of β-Hex activity in the supernatant moderately enhanced cross-correction, as shown by the 2-fold higher intracellular MUG-related enzymatic activity measured in SD cross-corrected cells (Fig. 4C), to reach up to 20% of WT activity. Of note, DEAE-cellulose chromatography showed the presence of HexB, HexI and HexA in all cross-corrected SD cells, with an improved rescue of enzymatic activity in SD cells exposed to the supernatant from LV.mAB-transduced SD cells as compared to WT UT cells, further confirming that enzyme over-expression enhances metabolic cross-correction of SD cells (Fig. 4D). The 30–40% reduction of GM2 storage detected in cross-corrected SD cells exposed to the supernatant containing physiological or supra-physiological levels of β-Hex activity (Fig. 4E–F) suggested that i) in this experimental *in vitro* setting the presence of 10–20% of normal enzyme ameliorates SD pathology; ii) the transgenic enzyme delivered by the bicistronic LV is as functional as the native counterpart. To further confirm these data, we analysed the sphingolipid pattern of untreated SD and cross-corrected neuronal/glial progeny by incubating SD NPCs in the presence of H^3-sphingosine for 48 h before adding the supernatant collected from donor cells. Thin layer chromatography (TLC) and quantification of radioactive bands showed a modest (< 10%) reduction in the content of GM2 but a much stronger reduction (30–60%) in the content of its asialo form GA2 in cross-corrected cells as compared to SD UT cells, with a clear advantage observed in the

presence of enzyme-enriched supernatant (Fig. 4G–H). The discrepancy in GM2 reduction observed by TLC as compared to immunofluorescence with the anti-GM2 antibody (Fig. 4E) may reflect the peculiarities and intrinsic limitations of these very different assays in capturing the complex ganglioside metabolism occurring in neural cell types.

Collectively, these data support the occurrence of GM2 clearance by supernatants from WT and transduced cells (with an advantage of the latter), indicating that the functional transgenic enzyme is secreted, recaptured by SD cells, and correctly delivered to lysosomes.

2.5. Efficient transduction and enzymatic rescue of murine HSPCs by bicistronic LVs

The optimization of gene transfer protocols ensuring the production and secretion of (supra) physiological HexA levels from HSPCs and progeny is mandatory to exploit the potential of autologous HSC GT approaches for GM2 gangliosidosis. To this end, we tested the efficacy of bicistronic LVs in achieving safe β-Hex rescue/overexpression in lineage negative (Lin-) HSPCs isolated from the BM of SD mice.

We transduced Lin- HSPCs with the different LVs at MOI 50. Transduced cells were plated in a methylcellulose-based medium for the colony forming cell (CFC) assay. The leftover was plated for differentiation in liquid cultures (LC). Fourteen days later, colonies were counted and LC were collected to perform VCN and β-Hex enzymatic activity. All LVs proficiently transduced Lin- HSPCs without evident toxicity, as shown by consistent VCN (range 2–6; Fig. 5A) and similar numbers of colonies (Fig. 5B) detected in all the conditions. MUG- and MUGS-related enzymatic activity was rescued to WT levels in SD cells transduced with LV.mB + LV.mA, LV.mAB, and LV.hAB (Fig. 5C–D; LC and CFC). The chromatographic profiles of SD cells transduced with LV.mB or the co-delivery of LV.mA + LV.mB showed the persistence of a consistent HexI peak, which is absent in physiological conditions (WT UT) (Fig. 5E–H; Suppl. Table 1). In contrast, LV.hAB-transduced SD cells showed a pattern of isoenzyme composition resembling the physiological counterpart, with a consistent presence of HexA and reduced formation of Hex I (Fig. 5I; Suppl. Table 1). This rescue was present but less evident in SD cells transduced with LV.mAB, which lack HexI but still show an unbalanced HexA/HexB ratio in favour or HexA (Fig. 5J; Suppl. Table 1).

These results showed the efficacy of bicistronic LVs in achieving effective reconstitution of β-Hex activity and close to normal isoenzyme composition, and suggest their potential advantage as compared to the co-delivery of monocistronic LVs in a clinically relevant cell type for prospective gene therapy approaches.

2.6. Enhancement of β-Hex activity in human neural and hematopoietic cells

We next assessed whether bicistronic LVs were effective and safe in clinically-relevant human cell types, namely neurons/glial cells and CD34 + HSPCs, in view of their potential clinical use for *in vivo* and/or *ex vivo* GT approaches.
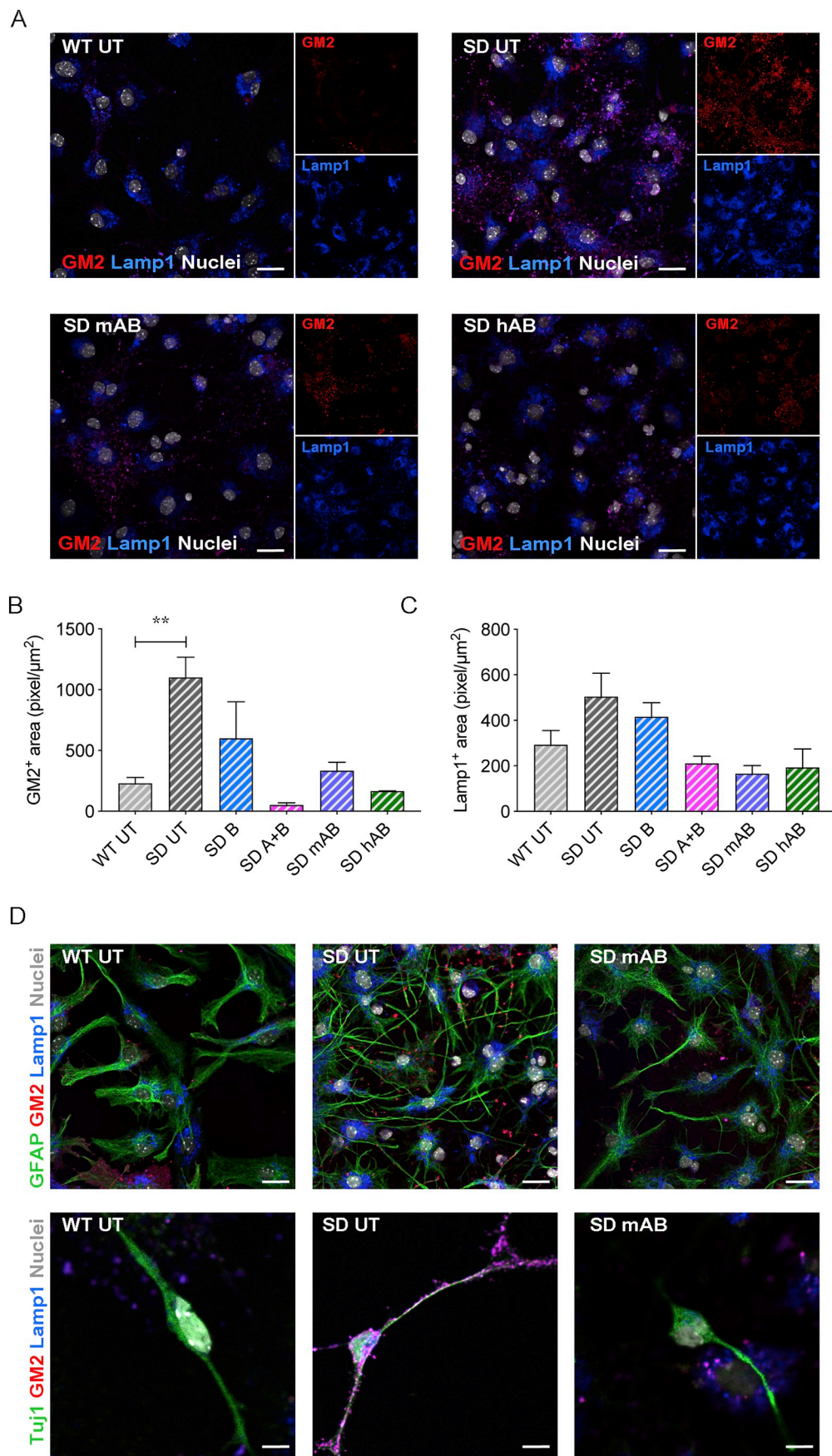
Fig. 3. GM2 storage and lysosomal expansion in SD neural progeny.

Representative immunofluorescence pictures (A) and quantification of immunoreactive area (B–C) showing GM2 storage and Lamp1 expression in SD UT differentiated cells and rescue to physiological levels (WT UT) in LV-transduced SD cells (SD mAB, SD hAB). In A: GM2, red; Lamp1, blue; Nuclei counterstained with Hoechst (grey, pseudocolor). Magnification: 40×. Scale bar, 50 μm. Data in B–C are the mean ± SEM, n = 3 experiments, 3 coverslips/experiment. **p < .01 *vs.* WT, One Way Anova followed by Kruskal-Wallis post-test. (D) Representative immunofluorescence confocal merged pictures showing GM2 expression (red) in astrocytes (GFAP, green) and neurons (TUJ1, green) of SD UT differentiated cells and rescue to physiological levels (WT UT) in LV.mAB-transduced SD cells. Scale bar, 50 μm (upper panels) and 10 μm (lower panels). (For interpretation of the references to colour in this figure legend, the reader is referred to the web version of this article.)
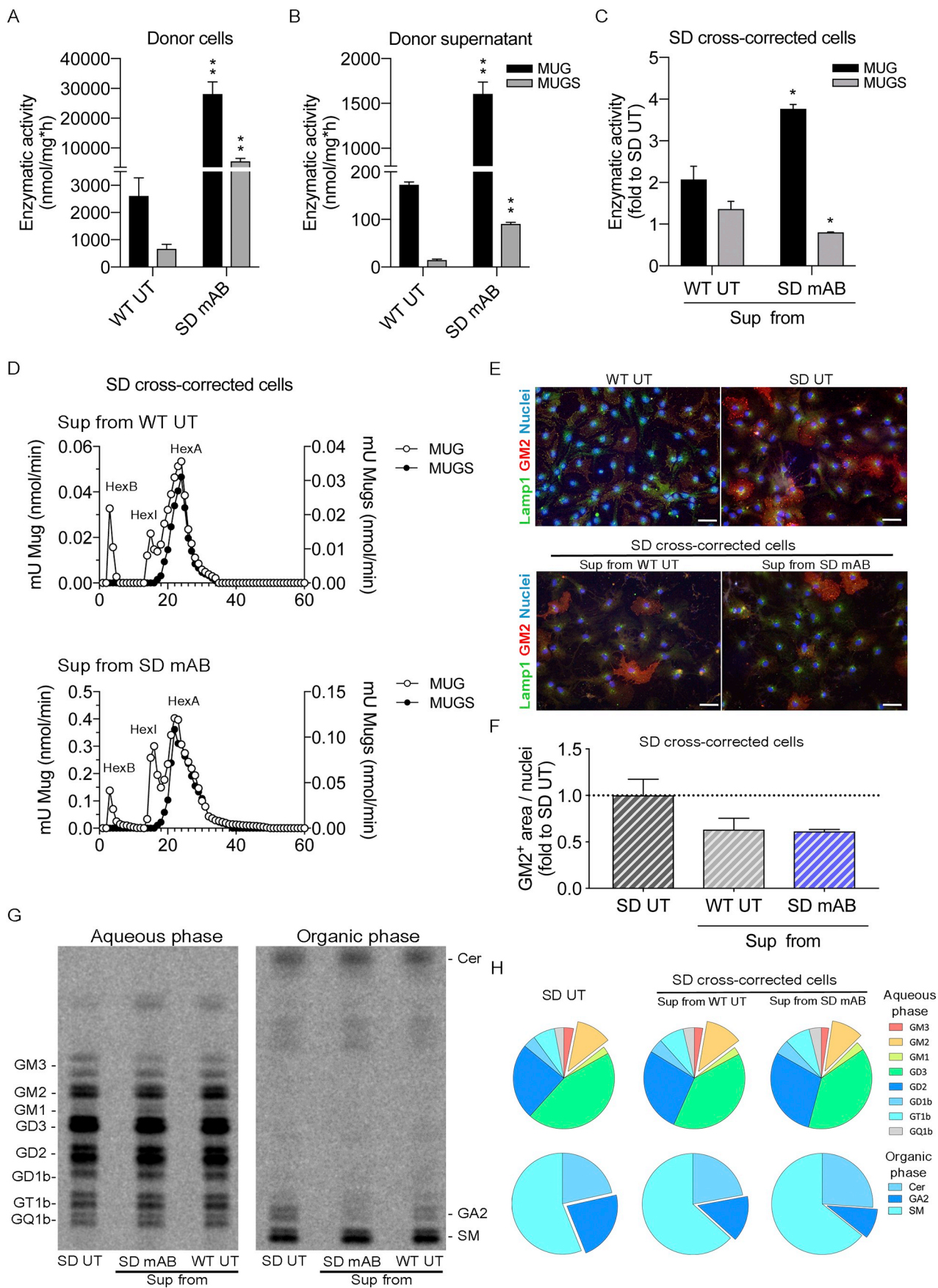
(caption on next page)

Fig. 4. Metabolic cross-correction of SD NPCs and progeny.
(A–B) Supraphysiological enzymatic activity in the cell pellet (A) and supernatant (Sup; B) of LV.mAB-transduced SD differentiated cells as compared to WT UT counterparts (*donor cells*) assessed by measuring MUG- and MUGS-related enzymatic activity. Unpaired Student *t*-test, ** p < .01 *vs.* WT UT (C) Enhanced MUG-related enzymatic activity in cross-corrected SD cells exposed to the Sup of LV.mAB-transduced (enzyme overexpressing) donor cells as compared to those exposed to the Sup of WT UT counterparts. Hex activity is expressed as fold to SD UT. Data are the mean ± SEM, n = 2 independent experiments. Unpaired Student *t*-test, * p < .05 *vs.* WT UT (D). DEAE chromatography showing the presence of HexA, HexB, and HexI isoforms in SD cross-corrected cells exposed to the Sup of WT UT or LV.mAB-transduced SD cells. Enzymatic activity (expressed as nmol/min; mU MUG on the left and mU MUGS on the right) and fraction number (0.5 ml) are plotted on the y and x axis, respectively. (E–F) Representative immunofluorescence pictures (E) and quantification of immunoreactive area (F; normalized on total nuclei) showing a 30–40% reduction of GM2 storage in SD cross-corrected cells. In E: GM2, red; Lamp1, green; nuclei counterstained with Hoechst (blue); magnification: 20×. Scale bar, 50 μm. Data in F are expressed as fold to SD UT and represent the mean ± SEM. n = 2 independent experiments. (G–H) Representative digital autoradiography (G) and quantification (H) of radioactive lipids obtained from SD UT or SD cross-corrected cells. Data in H are expressed as percentage of radioactivity (DPM/mg prot) of the single species on the total radioactivity associated with gangliosides and neutral sphingolipids, respectively. (For interpretation of the references to colour in this figure legend, the reader is referred to the web version of this article.)

We differentiated human induced pluripotent stem cell (iPSCs) - obtained by reprogramming of healthy donors (HD) fibroblasts - into NPCs and differentiated progeny using a protocol that generates mixed populations of neurons, astrocytes, and oligodendrocytes at different stages of differentiation/maturation (Frati et al., 2018). Seven days after plating, we exposed NPC-derived progeny to LV.hAB (MOI 2 and MOI 5; overnight incubation). Cultures were grown for additional 7 days in order to promote neuronal and glial differentiation and allow LV integration and transgene expression. Cultures were collected at day (d) 14 for molecular and biochemical analysis.

LV.hAB proficiently transduced hiPSC-derived neural progeny in a dose-dependent manner. The high VCN (range 20–30) obtained in LV-transduced cell populations using these relatively low MOIs reflects the presence of a variable amount of intracellular non-integrated vector in transduced cells, which is expected since these cells do not actively proliferate in these culture conditions (≈10% of proliferating cells at d14 of differentiation) (Frati et al., 2018). The average composition of NPC-derived cultures at d14 is: ≈ 15–20% neurons (TUJ1), 5–10% astrocytes (GFAP), 10–20% of oligodendrocytes (CNPase), 30–40% of neural progenitors (nestin+, A2B5+) (Frati et al., 2018). By qualitative immunofluorescence analysis we observed similar cell type composition and neuronal/glial morphology in UT and LV-transduced cultures (Fig. 6A). LV-transduced cells display a dose-dependent increase of β-Hex activity (up to 3 and 6-fold the normal levels, respectively, at MOI 2 and MOI 5; Fig. 6B), with a physiological MUG/MUGS ratio (≈11:1 and ≈10:1 in HD- and LV-transduced NPCs, respectively). The higher enzymatic activity measured in the supernatant of LV.hAB-transduced human NPC progeny as compared to untransduced counterparts (Fig. 6C and Suppl. Fig. 3) point to the potential advantage of transgene overexpression in enhancing the availability of β-Hex in the extracellular space in the context of *in vivo* gene therapy platforms. Importantly, the chromatographic profile of LV-transduced cells closely resembled the physiological counterpart (NPCs UT: HexB ≈ 47%; HexI ≈ 5%; HexA ≈ 48% of total Hex activity; LV.hAB NPCs: HexB ≈ 43%; HexI ≈ 15%; HexA ≈ 42% of total Hex activity) (Fig. 6D–E; Suppl. Table 1). Overall, these data suggest that LV.hAB-mediated transduction and β-Hex overexpression are well tolerated by iPSC-derived neural progeny and result in efficient production and secretion of functional HexA.

We used commercially available CD34+ HSPCs isolated from healthy donors (n = 2; donor#1 and donor#2), which underwent one round of transduction using LV.hAB (MOI 100) according to described protocols (Scaramuzza et al., 2013; Ungari et al., 2015). The VCN measured in LV-transduced HSPC progeny after 14 days of differentiation in liquid cultures (LC) was 0.66 (donor #1) and 0.42 (donor #2), in line with previous data (Scaramuzza et al., 2013). LV-transduced cells displayed a detectable increase of β-Hex activity (≈2-fold and ≈1.6-fold the HD level for MUG- and MUGS-related activity, respectively; Fig. 6F), a physiological 10:1 MUG/MUGS ratio (8:1 in UT CD34+ cells), and a normal chromatographic profile (Fig. 6G–H). In fact, LV.hAB-transduced cells display levels of HexB (≈52% of total Hex activity), HexI (≈11% of total Hex activity), and HexA (≈37% of total

Hex activity) comparable to those found in CD34+ UT cells (HexB ≈52%; HexI ≈11%; HexA ≈ 37%; Suppl. Table 1). Overall these results provide proof of concept of the feasibility and efficacy of using bicistronic LVs to achieve safe β-Hex overexpression in human HSPCs.

2.7. Rescue of enzymatic activity in SD fibroblasts by bicistronic LV.hAB

We sought to obtain proof of concept of LV.hAB-mediated rescue of enzymatic activity and isoenzyme composition in fibroblasts (hFF) derived from a SD patient (healthy donor –HD- fibroblasts were used as controls). SD fibroblasts were incubated overnight with LV.hAB (MOI 10 and MOI 20) and sub-cultured for 2 passages before being collected for molecular and biochemical analysis.

The VCN measured in LV.hAB-transduced SD fibroblasts ranged between 0.5 and 2.

LV-transduced SD fibroblasts displayed full rescue of β-Hex activity (Fig. 7A), a 8:1 MUG/MUGS ratio, and a physiological isoenzyme composition (HD UT: HexB ≈40%; HexI ≈20%; HexA ≈40% of total Hex activity; SD LV.hAB: HexB ≈23%; HexI ≈20%; HexA ≈57% of total Hex activity) (Fig. 7B–D; Suppl. Table 1). Western Blot analysis revealed mature expression of the HexA and HexB proteins in LV.hAB-transduced SD fibroblasts (Fig. 7E) with a pattern of α- and β-subunit composition comparable to that observed in HD UT counterparts (Suppl. Fig. 4).
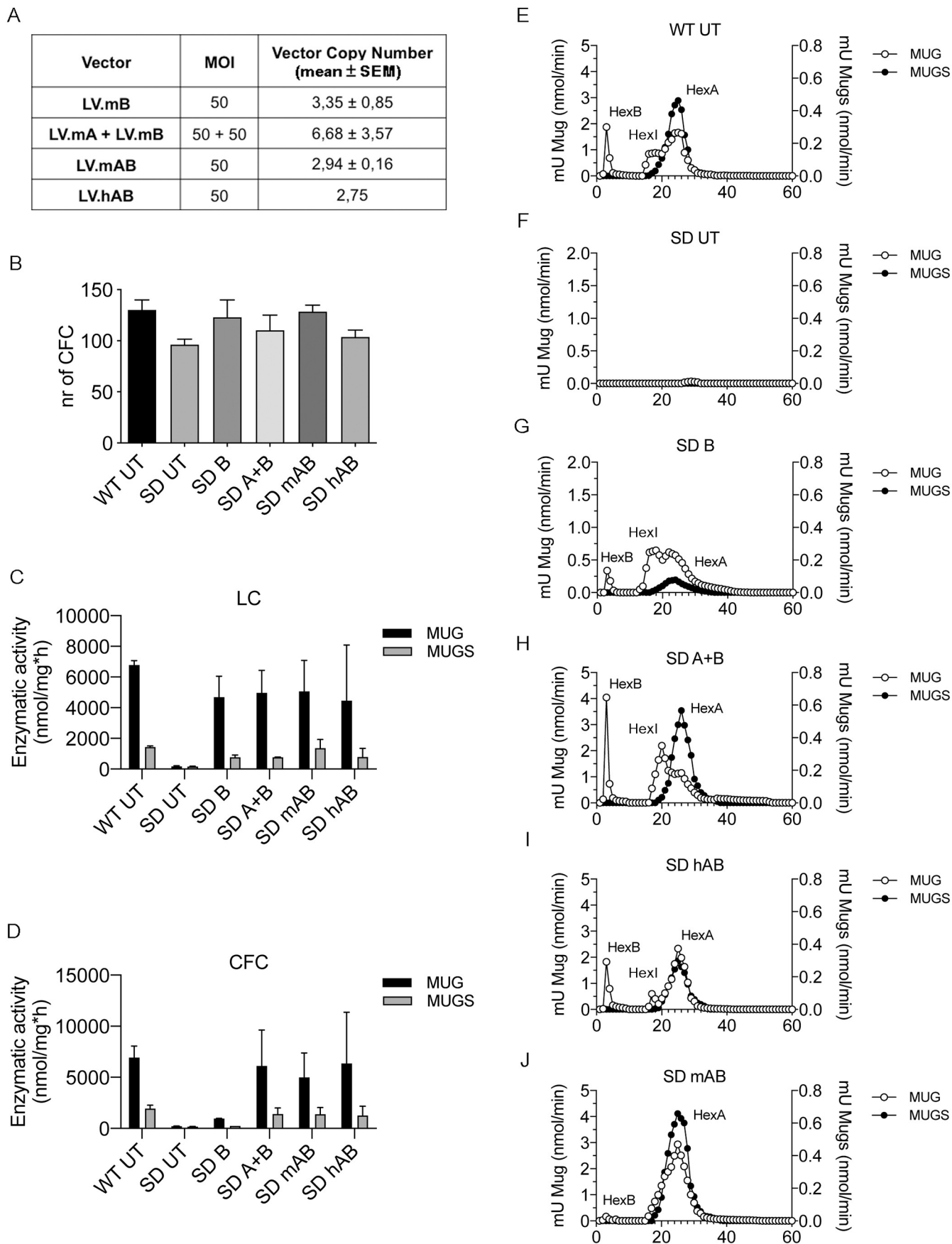
Importantly, LV.hAB-mediated enzymatic rescue led to clearance of GM2 storage, which is present in untreated SD fibroblasts (Fig. 7F).

Collectively, these results indicate that the bicistronic LV.hAB drives the synthesis and secretion of functional β-Hex enzyme in SD fibroblasts, highlighting its biological efficacy in a patient-derived cell type.

3. Discussion

Gene therapy (GT) is a promising approach to ensure a steady supply of β-Hex to CNS and other affected tissues potentially for the recipient's lifetime, with the capacity to comprehensively address GM2 gangliosidosis pathology. Hematopoietic stem cell gene therapy (HSC GT), in which autologous HSPCs are engineered with LVs to overexpress a functional enzyme, provides benefit in a similar LSD, metachromatic leukodystrophy (Biffi et al., 2013; Sessa et al., 2016), supporting the rationale for applying a similar approach to GM2 gangliosidosis. Prospectively, coupling the benefit of HSC GT with the timely enzymatic supply to CNS tissues provided by LV-mediated intracerebral (IC) GT is expected to provide a synergistic effect (Ricca et al., 2015). The experimental work described here contributes to the prospective clinical development of such approaches by addressing key and still unexplored feasibility, efficacy, and safety issues related to the (over)expression of a functional β-Hex enzyme using optimized bicistronic LVs in relevant murine and human neural and hematopoietic cell types that are target (neurons/glia) or effector cells (HSPCs) in *in vivo* and *ex vivo* GT approaches.

The peculiar biological features, coupled to scalable manufacture for clinical applications, make LVs safe and effective vehicles in the

A

Vector	MOI	Vector Copy Number (mean ± SEM)
LV.mB	50	3,35 ± 0,85
LV.mA + LV.mB	50 + 50	6,68 ± 3,57
LV.mAB	50	2,94 ± 0,16
LV.hAB	50	2,75

(caption on next page)

Fig. 5. Transduction of mono- and bicistronic LVs in murine HSPCs results in rescue of enzymatic activity and isoenzyme composition.
(A) VCN values in LV-transduced HSPCs (MOI 50 or 50 + 50 for co-delivered monocistronic LVs). Values are the mean ± SEM; n = 2–3 independent experiments; 3–4 samples/group. (B) Colony forming cell (CFC) assay shows similar number of colonies in all the conditions tested. $p > .05$ *vs.* WT UT, One-way Anova followed by Dunnet's post-test. (C–D) Rescue of MUG- and MUGS-related enzymatic activity to physiological levels (WT UT) in LC (C) and colonies (D) generated from SD HSPCs transduced with LV.mHexb + LV.mHexa, LV.mAB, and LV.hAB. (E–J) DEAE chromatography performed on LC from untransduced HSPCs (WT and SD UT; E, F) and LV-transduced SD HSPCs (LV.mAB, LV.hAB) shows the presence of HexA and HexB isoforms and a strong reduction of HexI in LV.hAB- and LV.mAB-transduced HSPCs (I–J). HexI is still present in SD HSPCs transduced with LV.mB (G) or with the co-delivered monocistronic LVs (LV.mA + LV.mB; H). Enzymatic activity (expressed as nmol/min; mU MUG on the left and mU MUGS on the right) and fraction number (0.5 ml) are plotted on the y and x axis, respectively.

context of *in vivo* and *ex vivo* GT approaches for LSDs, as suggested by pre-clinical studies (Ungari et al., 2015; Ricca et al., 2015) and results of recent Phase I/II clinical trials (Biffi et al., 2013; Sessa et al., 2016). Importantly, the large LV cargo capacity (Palfi et al., 2014; Grieger and Samulski, 2012) may overcome the issue of vector co-delivery or the need of developing small size chimeric proteins, facilitating the development of GT strategies for GM2 gangliosidosis. Based on these premises, we developed bicistronic LV constructs in which the murine and human genes coding for the α- and β-subunits are linked by a P2A self-cleaving peptide, which allows for stoichiometric and concordant expression of the two genes (Szymczak-Workman et al., 2012). In order to ameliorate the stability of the transcript and improve enzyme expression, we took advantage of codon optimization. Indeed, recoding the transgene to optimize transcription and translation has already been demonstrated to improve LVs titers as well as protein production and the efficacy of therapies, *i.e.*, for chronic granulomatous disease, haemophilia A and B, SCID, GLD and MLD (Biffi et al., 2013; Ungari et al., 2015; Chiriaco et al., 2014; Cantore et al., 2015).

Our results show safe and effective bicistronic LV-mediated transduction of murine SD NPCs and differentiated progeny, a cellular model that recapitulates the pattern of β-Hex expression and isoenzymatic composition and display consistent GM2 storage and lysosomal expansion, two main LSD pathological hallmarks (Ballabio and Gieselmann, 2009). All LVs proficiently transduced SD NPCs, resulting in multiple copies of integrated LV genome/cell (VCN). The comparable VCN measured in cells transduced with either bicistronic LVs (MOI 50) or co-delivered monocistronic LVs (MOI 50 ± 50) may reflect an early counter selection of the double-transduced cells achieving an excessive vector load. The use of bicistronic LVs has the potential to decrease the LV dose needed for effective transduction, further improving the safety profile. All LV-transduced NPCs cells maintained normal proliferation and multipotency over time *in vitro*, confirming previous data showing safe LV-mediated gene transfer in NPCs derived from LSD murine models (Neri et al., 2011; Lattanzi et al., 2010).

Our comprehensive molecular and biochemical analysis showed that bicistronic LVs outperform the co-delivered monocistronic LVs in achieving stoichiometric expression of the α- and β-subunits in SD NPCs and progeny. Indeed, while the co-delivery of monocistronic LVs - and even the single delivery of LV.mB - was sufficient to boost β-Hex activity, only transduction with bicistronic LVs resulted in close-to-physiological MUG- and MUGS- related activity and balanced HexA/HexB expression. Importantly, transduction with bicistronic LV.hAB resulted in supranormal levels of β-Hex activity and correct isoform expression in iPSC-derived human neurons/glial cells derived from healthy donors. We have previously shown that therapeutic LVs mediated enzymatic rescue of neurons and glial cells derived from MLD patients (Meneghini et al., 2017) and GLD NHP (Meneghini et al., 2016). The formation of mature HexA and HexB transgenic proteins in LV.hAB-transduced murine SD NPCs and progeny as well as in SD patient-derived fibroblasts suggests the biological efficacy of the bicistronic LV.hAB in SD pathology. In addition, these data support the advantage of this bicistronic construct (hexb-P2A-hexa) as compared to the one described previously (hexb-IRES-hexa), which led to an excess of ββ at the expenses of αβ formation in SD fibroblasts (Arfi et al., 2005). Based on these premises, we expect a similar safety and efficacy profile in SD patient-derived neural cells, which should be ultimately tested as they

represent the target of prospective intracerebral GT approaches.

The production and secretion of (supra) physiological HexA from HSPCs and progeny is mandatory to exploit the potential of autologous HSC GT for the treatment of GM2 gangliosidosis. We leveraged on a LV GT platform that has been effectively applied to (over)express therapeutic transgenes (including lysosomal enzymes) in HSPCs, both in pre-clinical studies (Ungari et al., 2015; Visigalli et al., 2010) and in the context of autologous *ex vivo* HSC GT Phase I/II clinical trials in patients with MLD (Biffi et al., 2013; Sessa et al., 2016), WAS (Aiuti et al., 2013; Ferrua et al., 2019), β-thalassemia (Marktel et al., 2019) and MPS I (ClinicalTrials.gov Identifier: NCT03488394). Our results extend the applicability of this platform to bicistronic LVs expressing the α- and β-subunits of β-Hex enzyme, which showed a clear advantage as compared to co-delivered monocistronic LVs in achieving safe and effective reconstitution/moderate overexpression of β-Hex activity and amelioration/normalization of isoenzyme composition in both murine (Lin-) SD HSPCs and human CD34 + cells from healthy donors. As compared to neural cells, HSPCs are poorly permissive to LV gene transfer, due to quiescence and the presence or enhanced expression of innate or adaptive restriction factors acting at different steps of the transduction pathway (Santoni de Sio et al., 2006; Wang et al., 2014). Robust gene transfer thus requires cell pre-stimulation with activating cytokines and high concentrations of LV with high specific infectivity. Our data showing VCN < 1 in CD34 + cells transduced with LV.hAB at MOI 100 (one round of transduction) are in line with previous results obtained by using lab-grade and clinical-grade LV preparations (Scaramuzza et al., 2013). Current efforts toward improvement of transduction protocols include the use of new drugs able to counteract restriction factors and enhance gene transfer (Wang et al., 2014; Petrillo et al., 2015; Zonari et al., 2017; Petrillo et al., 2018; Heffner et al., 2018) and optimized culture conditions to increase the yield and fitness of transduced cells (Boitano, 2011; Wagner et al., 2016; Cutler et al., 2013; Watts et al., 2013; Fares et al., 2017). Some of these improvements have been introduced in recent experimental clinical protocols and could become standard procedure in prospective clinical development of HSC GT for GM2 gangliosidosis.

The therapeutic benefit expected by *in vivo* and/or *ex vivo* GT approaches for LSDs not only rely on the direct correction of endogenous CNS cells or pervasive replacement of tissue-resident myeloid cells with HSPC-derived functional counterparts, but also on the release of part of functional enzyme by genetically modified cells for its uptake by neighbouring enzyme-deficient cells (metabolic cross-correction). The extent of secretion and reuptake varies among the different lysosomal enzymes and in different cells types (Markmann et al., 2015; Klein et al., 2009). Previous works reported cross-correction of SD fibroblasts (Arfi et al., 2005), but limited information is available for neural and hematopoietic cells (Ohsawa et al., 2005; Oya et al., 2000; Tsuji et al., 2005). We detected 10–20% of normal β-Hex activity in cross-corrected SD neurons/glia cultures exposed to supranormal enzymatic activity. This rescue was sufficient to achieve a 30–60% reduction of GM2 and GA2 storage in these *in vitro* models, as evaluated using different assays. Optimization of LV and transgene design may improve vector particle distribution and enhance enzyme bioavailability in the context of GT approaches (Sorrentino et al., 2013; Gleitz et al., 2018). Tailored experiments testing β-Hex activity in the CSF, CNS, PNS, and peripheral organs of SD mice undergoing *in vivo* and/or *ex vivo* GT approaches
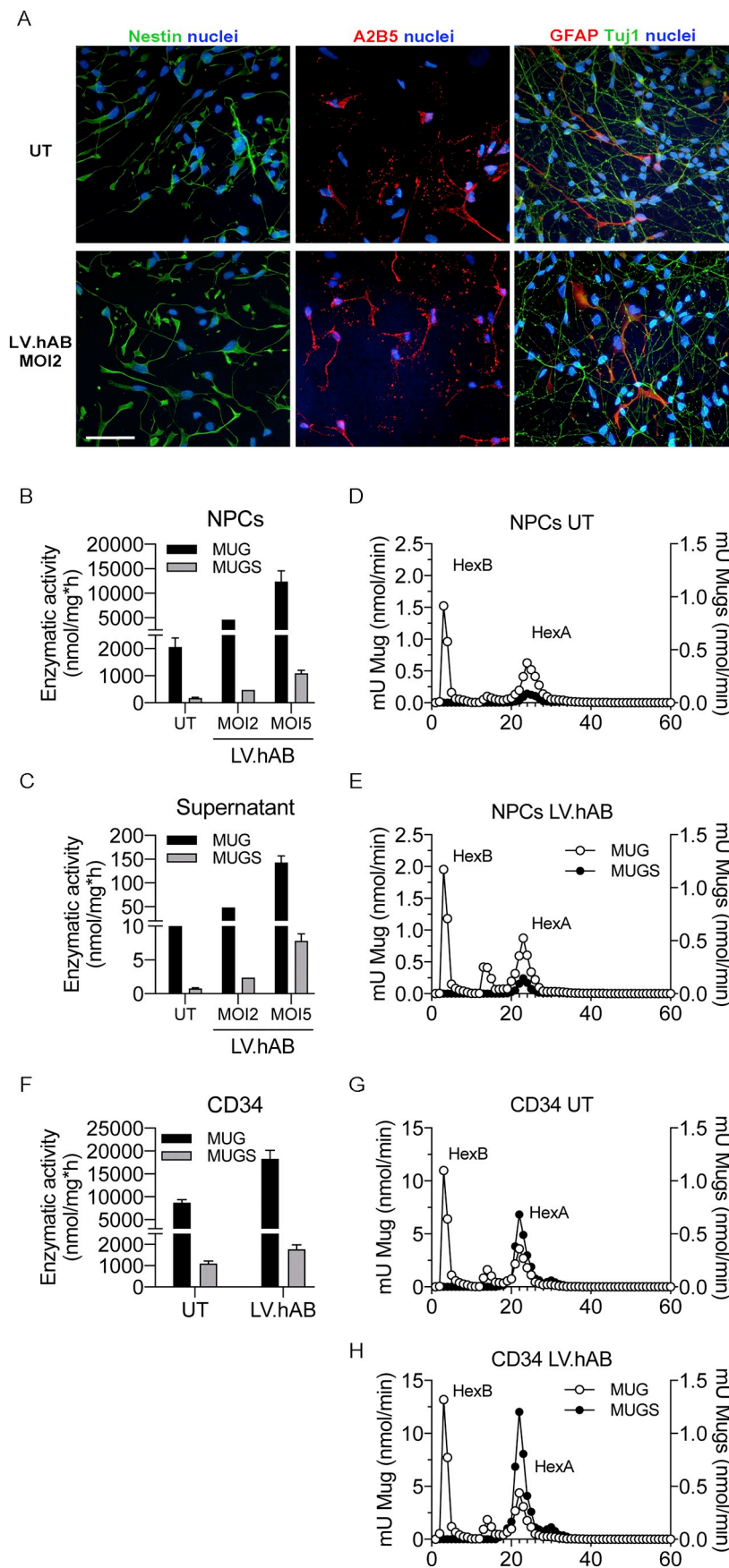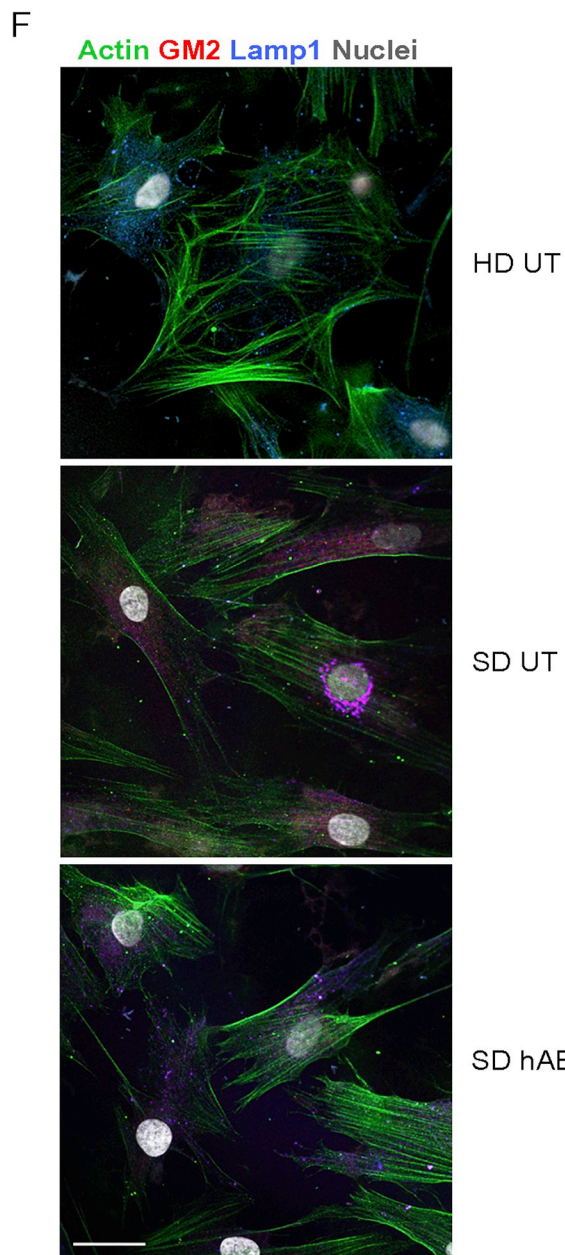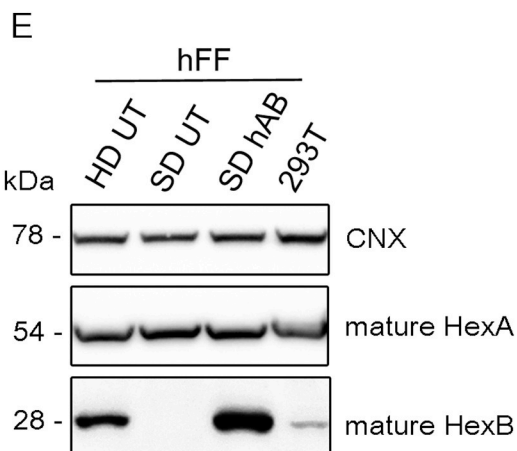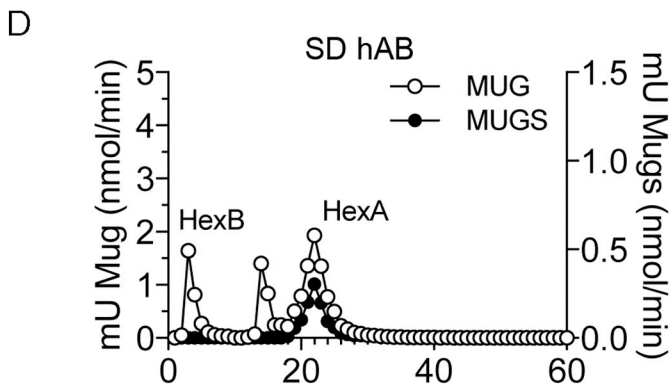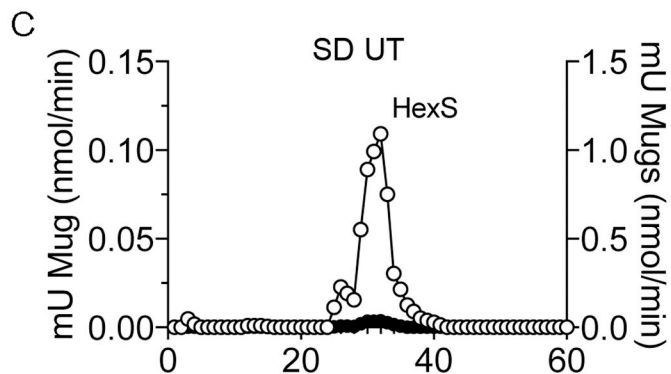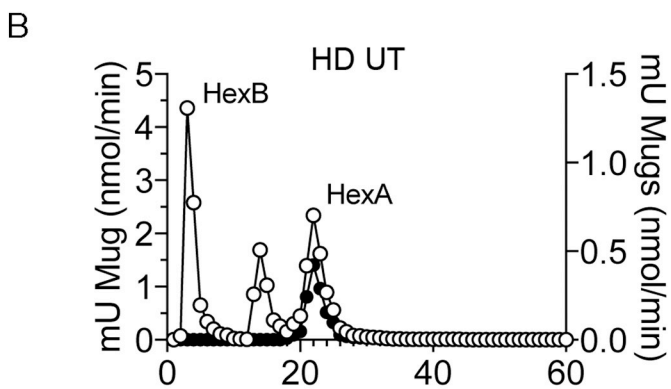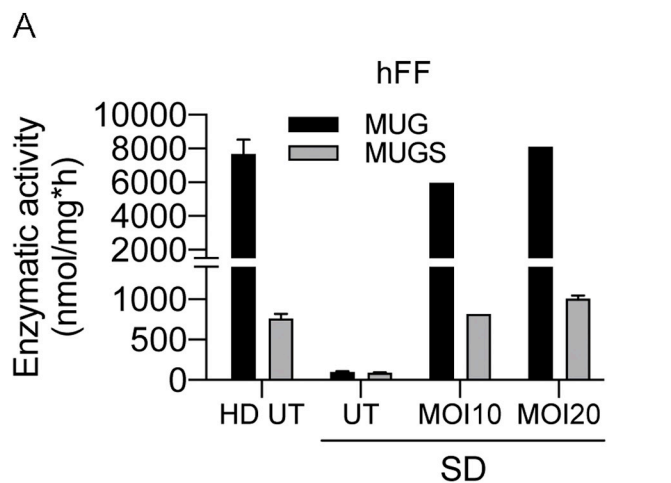
Fig. 6. Bicistronic LV.hAB rescues β-Hex activity in human neural and hematopoietic stem/progenitor cells from healthy donors.

(A) Representative immunofluorescence confocal pictures showing similar cell type composition in neural progenitors (Nestin, green; A2B5, red), neurons (TUJ1, green), and astrocytes (GFAP, red) in UT and LV-transduced hiPSC-derived neural cultures. Scale bar, 50 μm in all panels (shown in the bottom left panel). (B–C) LV.hAB-transduced iPSC-derived neurons/glial cells display dose-dependent increase of MUG- and MUGS-related enzymatic activity in the cell lysate (B) and in the supernatant (C) as compared to untreated (UT) counterparts. MOI, multiplicity of infection. (D–E) DEAE chromatography shows comparable isoenzyme composition in LV.hAB-transduced human NPCs (E; MOI 2) as compared to UT counterparts (D). (F) LV.hAB-transduced CD34+ HSPCs cells display 1.5- to 2-fold increase in MUG- and MUGS-related enzymatic activity as compared to UT counterparts. (G–H) DEAE chromatography performed on LC from UT (G) and LV.hAB-transduced CD34+ cells (H) show comparable isoenzyme composition. (For interpretation of the references to colour in this figure legend, the reader is referred to the web version of this article.)

A

hFF

B

HD UT

C

SD UT

D

SD hAB

E

hFF

F

Actin GM2 Lamp1 Nuclei

(caption on next page)

13

Fig. 7. Bicistronic LV.hAB rescues enzymatic activity in SD fibroblasts.

(A) Transduction of SD patient–derived fibroblasts (hFF) with LV.hAB (MOI 10 and 20) rescues β-Hex activity to physiological levels. (B–D) DEAE chromatography shows comparable isoenzyme composition in LV.hAB-transduced SD hFF (MOI 20) and untransduced healthy donor hFF (HD UT). Enzymatic activity (expressed as nmol/min; mU MUG on the left and mU MUGS on the right) and fraction number (0.5 ml) are plotted on the y and x axis, respectively. (E) Western blot using anti-α- and anti-β- chain antibodies shows the presence of the mature HexA (54 kDa) and HexB protein (28 kDa) in HD UT and LV.hAB-transduced but not in untransduced SD hFF; human 293 T cells served as control. (F) Representative immunofluorescence confocal pictures showing GM2 storage and increased LAMP1 expression in SD UT fibroblasts, which are cleared or reduced in LV.hAB-transduced counterparts (MOI 20). Fibroblasts from HD are shown for comparison. GM2, red; Actin, green; Lamp1, blue. Nuclei are counterstained with Hoechst (white; pseudocolor). Magnification: 63×. Scale bar, 25 μm. (For interpretation of the references to colour in this figure legend, the reader is referred to the web version of this article.)

could definitely assess whether LV-transduced endogenous CNS cells and/or HSPC-derived myeloid progeny replacing the tissue resident microglia and macrophages secrete sufficient levels of β-Hex to ensure effective cross-correction and full metabolic rescue of endogenous enzyme-deficient neurons/glia of SD mice (and prospectively patients).

4. Conclusion

We here demonstrated the safe and effective profile of novel bicistronic LVs in driving robust β-Hex expression with preferred formation of a functional HexA (αβ) in SD murine NPCs, HSPCs and progeny, as well as in human SD fibroblasts, normal iPSC-derived neurons/glia, and CD34 + HSPCs. We expect that human SD HSPCs and neurons/glia could benefit even more from this approach for the sustained enzyme activity mediated by gene transfer that could restore cellular functions and promote the cross-correction of affected cells. Altogether, these findings provide a strong rationale for considering these bicistronic LVs as promising candidates for the clinical translation of *in vivo* and *ex vivo* GT approaches for GM2 ganglisidosis.

5. Material and methods

5.1. Lentiviral vectors

5.1.1. Cloning

In all lentiviral vectors (LVs) the expression of transgenes was driven by the human phosphoglycerate kinase (hPGK) promoter. Briefly, hexa and hexb murine cDNAs were inserted in the backbone of LV using BamH1-Sal1 unique restriction sites. The plasmids codifying for LV.mAB and LV.hAB were synthetized by Gene Script (New Jersey, USA) using the murine and the human codon-optimized sequence. Each plasmid encodes for the cDNA of murine or human hexb, P2A sequence (5′- GGAAGCGGAGCTACTAACTTCAGCCTGCTGAAGCAGGCTGGAGAC GTGGAGGAGAACCCTGGACCT-3′), and murine or human hexa, in this order.

5.1.2. Production and titration

VSV-pseudotyped third-generation LVs were produced by transient four-plasmid cotransfection into 293T cells and purified by ultracentrifugation, as described (Amendola et al., 2005; Vigna et al., 2005). Expression titers of vectors were estimated on human cells (293T) by limiting dilution and calculation of the copies of integrated vector (VCN) per cell by quantitative PCR. Specifically, titer was calculated as VCN × number of plated cells × dilution of vector. Vector expression titer was expressed as transducing units (TU)/ml. Vector particle was measured by HIV-1 gag p24 antigen immunocapture (NEN Life Science Products). Vector infectivity was calculated as the ratio between titer and particle and expressed as TU/ng of p24 (Titer/p24).

Titer and infectivity for the different LVs are the following:

LV.mA – Titer: $0.68*10^9$ TU/ml; Infectivity: $3.78*10^4$ TU/ng
LV.mB – Titer: $1.15*10^9$ TU/ml; Infectivity: $7.47*10^4$ TU/ng
LV.mAB – Titer: $1.66*10^9$ TU/ml; Infectivity: $3.31*10^4$ TU/ng
LV.hAB – Titer: $2.69*10^9$ TU/ml; infectivity: $4.41*10^4$ TU/ng

5.2. Establishment of murine NPC lines

Murine NPC cell lines were established as previously described (Gritti et al., 2009). Briefly, 3-month-old WT and SD mice were anaesthetised by intraperitoneal injection of Avertin (2,2,2-Tribromoethanol; 0.25 mg/g body weight). Brains were removed and transferred in a Petri dish containing PBS + Glucose (0,6%) + Penicillin/Streptomicin (P/S) (1%). The olfactory bulbs were removed, a coronal slice comprising the periventricular subventricular zone (SVZ) of the forebrain lateral ventricles was cut and the periventricular tissue was carefully dissected. After enzymatic digestion, tissue was dissociated and single cells were plated in DMEM/F12 (1:1) medium supplemented with EGF2 and FGF2 (20 ng/ml; growth medium) to generate primary neurospheres that were collected and serially passages to establish NPC cultures. We established independent cell lines from the SVZ of SD and WT mice (n = 2 for each genotype). For all the experiments, we used serially passaged NPCs (passage 5–15). All lines underwent functional characterization (self-renewal, proliferation, and multipotency), as described below.

5.3. Lentiviral vector-mediated gene transfer in NPCs

Serially subcultured NPCs (passages 5–10) were plated in growth medium (proliferating conditions) in 6-well plates (30,000 cells/cm^2). Eight hours after plating cells were incubated overnight with LVs at MOI 50. LV-containing medium was then removed, fresh medium added, and cells incubated for additional 4–6 days to obtain neurospheres that were further subcultured to establish stable LV-transduced NPC lines. LV-transduced NPCs were analysed for their functional features before being used for the experiments.

5.4. Functional characterization of NPCs

5.4.1. Proliferation

Long-term proliferation of the bulk NPC cultures was assessed by generating growth curves, as previously described (Gritti et al., 2009). Briefly, we plated 2×10^5 viable cells in a 25 cm^2 flask (0 days *in vitro*-DIV) in growth medium. At each subculture passage (every 4–5 days) the total number of viable cells was counted, and 2×10^5 cells were replated under the same conditions. This procedure was repeated for at least 5 subculture passages. The estimated total number of cells was calculated by multiplying the amplification rate (total number of cells obtained at a given subculture passage/2×10^5) for the total number of cells obtained at the previous passage. The total number of cells (in log10 scale) was plotted against the DIV. Data were interpolated using a linear regression model and best fitted the following equation: y = a + bx, where y is the estimated total number of cells (in log scale), x is the time (DIV), *a* is the intercept (constrain: 2×10^5), and b is the slope. The best-fit value, the standard error, and the 95% confidence intervals of the slope for each dataset were calculated. The slope values were then compared using one-way ANOVA followed by Dunnet's multiple comparison test. Statistical significance was accepted with $P \leq .05$.

5.4.2. Clonogenic assay

Serially passaged neurospheres were dissociated and cells were plated in growth medium (1000 cells/cm^2 in 48-well plates). The number of newly formed neurospheres in each well was counted after 7 days. The ratio between the number of neurospheres obtained and the number of plated cells (x100) is indicated as clonal efficiency.

5.4.3. Multipotency

Cells were induced to differentiate by progressive removal of growth factors. Serially passaged NPCs were plated (40,000 cells/cm^2) onto an adhesive substrate (matrigel) in growth medium for two days. The resulting population (*precursors*) was either collected for molecular and biochemical analysis or further induced to lineage commitment and differentiation by exposure to FGF2-containing medium for 48 h, followed by 5 days in a mitogen-free medium containing 2% FBS, to drive the differentiation into neurons and glia (*differentiated cells*). The percentage of neuronal and glial cells in differentiated cells was assessed by immunofluorescence analysis and quantification using lineage-specific markers.

5.5. Isolation and transduction of murine hematopoietic stem/progenitor cells (HSPCs)

Young adult mice (4–8 weeks) were sacrificed with CO_2, and bone marrow (BM) was harvested by flushing femurs, tibias, and humeri. Murine HSPCs were purified (lineage cell depletion kit, Miltenyi 130–090-858; LS columns, Miltenyi 130–042-401) and plated (100,000 cells/cm^2) in StemSpan serum-free medium (Stemcell 09650) supplemented with cytokines (mSCF, 5 ng/ml; hFlt3L, 10 ng/ml; mIL3, 10 ng/ml; TPO, 50 ng/ml; all from Peprotech) in the presence of LVs at MOI 50 for 12 h. After transduction, HSPCs were: i) washed, counted, and seeded at a density of 4000 cells/ml in semi-solid medium (murine Methocult, StemCell 03434). After 14 days, colonies were scored and counted (CFC assay); ii) plated in RPMI medium (Corning 15040CVR), 10% FBS (Euroclone ECS0180L), 1% P/S (Lonza 17-602E), 1% L-glutamine (Lonza 17-605E), and cytokines (mSCF, 5 ng/ml; hFlt3L, 10 ng/ml; mIL3, 10 ng/ml; TPO, 50 ng/ml; all from Peprotech), cultured for 14 days before being collected and analysed for VCN, enzymatic activity, and isoenzyme composition (liquid cultures, LC).

5.6. Human cells

Human cells were used according to the guidelines on human research issued by the San Raffaele Scientific Institute's Ethics Committee, in the context of the protocol TIGET-HPCT (approved 03.12.2009).

5.6.1. HSPCs

Human HSPCs from two healthy donors (umbilical cord blood-derived CD34 +) were purchased from Lonza (Verviers, Belgium; product code 2C-101). Cells (80,000 cells per condition) were pre-stimulated for 12 h with the standard CB-HSPCs cytokine cocktail (hIL-6, 20 ng/μl; hTPO, 20 ng/μl; hSCF, 100 ng/μl; hFlt3-L, 100 ng/μl) in StemSpan serum-free medium (StemCell Technologies, Vancouver, British Columbia, Canada) and then incubated with LV.hAB at MOI 100 overnight. Transduced HSPCs were plated in IMDM medium (Sigma Aldrich, St Louis, MO), 10% FBS (Euroclone, Pero, Italy), penicillin 100 U/ml and streptomycin 100 μg/ml, L-glutamine 2 mmol/l, and cytokines (hSCF, 300 ng/μl; hIL3, 60 ng/μl; hIL6, 60 ng/μl) and cultured for 14 days before being collected and analysed for VCN, enzymatic activity and isoenzyme composition (liquid cultures).

5.6.2. Induced pluripotent stem cell (iPSC)-derived neural progeny

The human iPSC lines used in this work are derived from the reprogramming of HD fibroblasts obtained by the Cell Line and DNA Bank of Patients affected by Genetic Diseases (code FFF0561980) or purchased from Invitrogen (code C0045C). The characteristics of the cell lines and the protocols to obtain iPSC-derived NPCs and neuronal/glial progeny have been previously described (Frati et al., 2018). All the cells used were mycoplasma-free (tested once every two weeks). Briefly, iPSC-derived NPCs were cultured in proliferating medium (NPCM; basal medium containing FGF2 and EGF), detached using Accutase and replated on Matrigel-coated dishes (20,000 cells/cm^2) in NPCM (d0). During the first 4 days after plating (d4) we gradually replaced NPCM with an increasing amount of differentiation medium (basal medium supplemented with 10 ng/ml PDGF-AA, 10 ng/ml NT3, 10 ng/ml IGF-1, 5 ng/ml HGF, and 60 ng/ml T3) to favour neural lineage commitment and differentiation. From d4 to d13 medium was changed every other day. At d7, cultures were incubated overnight with LV.hAB (MOI 2 and MOI 5) supplemented with 8 mg/ml Polybrene (Sigma-Aldrich, St. Louis, MO). Then, LV-containing medium was removed, and fresh medium added for additional 7 days. Cells were analysed at d14 for VCN, morphology and cell type composition, enzymatic activity and isoenzyme composition.

5.6.3. Fibroblasts

Skin fibroblasts derived from one SD patient and one healthy donor (HD) were obtained from the Cell Line and DNA Bank of Patients affected by Genetic Diseases (Institute Gaslini, Genova, Italy, http://www.gaslini.org). Fibroblasts were plated (10,000 cells/cm^2) in human fibroblasts medium (HFM): DMEM (Life Technologies), 10% Fetal Bovine Serum (Euroclone), 0.1 mM non-essential amino acids (Life Technologies), 1 mM Sodium Piruvate (Life Technologies), 2 mM L-Glutamine (Lonza), 100 U/ml penicillin/streptomycin (Lonza) supplemented with 8 mg/ml Polybrene (Sigma-Aldrich, St. Louis, MO). Cultures at ≈70% confluence were incubated with LV.hAB (MOI 10, MOI 20) overnight. LV-containing medium was then removed and fresh HFM added. Cells were collected 10 days after transduction and analysed for VCN, enzymatic activity, isoenzyme composition, and immunofluorescence.

5.7. Quantification of vector copy number (VCN)

Genomic DNA (gDNA) from human and murine cells was extracted from cellular pellets (Maxwell 16 Cell DNA purification kit, Promega), following the manufacturer instructions. gDNA was quantified by 260/280 nm optical density (OD) reading on the NanoDrop ND-1000 Spectrophotometer (Euroclone, Pero, Italy). The number of vector copies integrated in the host genome (vector copy number, VCN) was quantified by quantitative droplet dd-PCR, using the custom primers and probes listed below. VCN were normalized to genomic DNA content, which was assessed using the murine SEMA3A or the human TELO gene. VCN analysis by ddPCR involved quantification of target and reference loci through the use of duplex target and reference assays. In QuantaSoftTMsoftware, copy number was determined by calculating the ratio of the target molecule concentration to the reference molecule concentration, times the ploidy of reference species.

Murine endogenous gene primers and probes:
Sema3A primers/HEX probe set

- Forward primer: 5′-ACC GAT TCC AGA TGA TTG GC-3′
- Reverse primer: 5′-TCC ATA TTA ATG CAG TGC TTG C-3′
- HEX probe: 5′- (HEX) - AGA GGC CTG TCC TGC AGC TCA TGG-(BHQ-1) - 3′

Human endogenous gene primers and probes:
TELO primers/Vic-TAMRA probe set

- Forward primer: 5′-GGCACACGTGGCTTTTCG-3′
- Reverse primer: 5′-GGTGAACCTCGTAAGTTTATGCAA-3′
- Vic-TAMRA probe: 5′-TCAGGACGTCGAGTGGACACGGTG-3′

Transgene primers and probes:
HIV primers/FAM probe set

- Forward primer: 5′-TACTGACGCTCTCGCACC-3′
- Reverse primer: 5′-TCTCGACGCAGGACTCG-3′
- FAM probe: 5′-ATCTCTCTCCTTCTAGCCTC-3′

5.8. Immunofluorescence (IF)

Double-labelling immunofluorescence was performed as previously described (Martino et al., 2009). Cultures were fixed in 4% PFA, rinsed with PBS, incubated with blocking solution containing 10% normal goat serum (NGS) with or without 0.1% Triton X-100 (Sigma) in PBS for 1 h at RT and incubated o/n at 4 °C with primary antibodies diluted in blocking solution. After three washing in PBS of 5 min each, antibody staining was revealed using species-specific fluorophore-conjugated secondary antibodies diluted in PBS + 1% NGS for 1 h. Nuclei were counterstained with Hoechst (10 µg/ml in PBS, Thermofisher). Coverslips were mounted on glass slides using Fluorsave (Calbiochem). Samples incubated only with secondary antibodies were used as negative controls.

Primary antibodies: monoclonal anti-Tuj1 (1:500; Biolegend, 801202); polyclonal anti-Tuj1 (1:500; Biolegend, 802001); polyclonal anti-GFAP (1:1000; DAKO, ZO334); monoclonal anti-GFAP (1:1000; Millipore, MAB 3402); monoclonal anti-O4 (1:500; R&D, MAB 1326); monoclonal anti-GM2 (1:500; TCI EUROPE, A2576); polyclonal anti-Lamp1 (1:200; Abcam, AB24170); hybridoma anti-Lamp1 (1:300; DSHB, 1D4B); monoclonal anti-A2B5 (1:1000; Chemicon, MAB 312r); monoclonal anti Nestin (1:200; Millipore, MAB 353); rabbit anti-actin (1:500; Santa-Cruz, sc-1616r).

Secondary antibodies (all from Thermo Fisher Scientific): ALEXA 488 (1:1000; anti-rabbit A11008, anti-mouse A11001); ALEXA 546 (1:2000; anti-mouse A11039); ALEXA 633 (1:500; anti-rat A21094).

5.9. Image acquisition and quantification

Coverslips were visualized with a Nikon Eclipse E600 microscope and images were acquired at 20× or 40× magnification with Nikon DS Ri-2 camera, using NIS-Elements F imaging software (Nikon, Japan). Immunoreactive cells were counted in at least 5 non-overlapping fields in each sample (> 300 cells/sample) and expressed as a percentage on the total nuclei. Data are the mean ± SEM of two-three coverslips in three independent experiments. Images were analysed by the ImageJ software to quantify GM2 and LAMP1 signal intensity corresponding to immunopositive areas (expressed in pixels). UT samples were used for setting the threshold. The area was normalized on the number of nuclei in the same field. The merged images were obtained using the Volocity Software (v5.2.1; PerkinElmer- Improvision, Lexington, MA). Images were imported into Adobe Photoshop CS4 and adjusted for brightness and contrast.

Confocal images were acquired at 63× magnification with a Leica TCS SP8 confocal microscope and analysed with LasX software.

5.10. Real time RT-PCR

Total RNA was extracted from cells by RNeasy mini Kit (Qiagen, Hilden, Germany), following the manufacturer's instructions. Reverse transcription was carried out using 1 µg of total RNA and the Quantitect Reverse Transcriptase kit (Qiagen, Hilden, Germany). qPCR was performed in Optical 96-well Fast Thermal Cycling Plates (Applied Biosystem) on ViiATM 7 Real-Time PCR System (Applied Biosystem), using the following thermal cycling conditions: one cycle at 95 °C for 5 min, 40 cycles at 95 °C for 15 s and 60 °C for 1 min, using Universal PCR Master Mix (Applied Biosystems) and TaqMan Gene Expression Assays (Applied Biosystems). Commercial probes and primers are listed below. The SDS 2.2.1 software was used to extract raw data. Relative expression of mRNA for the target genes was calculated by the comparative CT ($\Delta\Delta$CT) method, using a housekeeping gene as control. Briefly, ΔCt was calculated for each sample as the Ct of the gene of interest minus the Ct of the normalizer (GAPDH). The $\Delta\Delta$Ct was then determined as the ΔCt of each sample minus the average of the ΔCt of controls. Finally, the fold change was expressed as 2ˆ(-$\Delta\Delta$Ct), for each sample.

PRIMERS AND PROBES		
Gapdh	Glyceraldehyde 3-phosphate dehydrogenase	Mm99999915_g1
mHex a	Murine Hexosaminidase α subunit	Mm00599877_m1
mHex b	Murine Hexosaminidase β subunit	Mm01282432_m1
mHex a c.o.	Murine codon-optimized Hexosaminidase α subunit	Custom
mHex b c.o.	Murine codon-optimized Hexosaminidase β subunit	Custom
hHex a c.o.	Human codon-optimized Hexosaminidase α subunit	Custom
hHex b c.o.	Human codon-optimized Hexosaminidase β subunit	Custom

5.11. β-Hexosaminidase activity and isoenzyme composition

Enzymatic activity and isoenzyme composition was determined in cell extracts as previously described (Martino et al., 2009; Martino et al., 2005; Martino et al., 2002; Martino et al., 1995) and briefly summarized here.

5.11.1. Cell extracts

Cells were harvested, washed in PBS and resuspended in 10 mM sodium phosphate buffer, pH 6.0, containing 0.1% (v/v) Igepal detergent (Sigma-Aldrich, St, Louis, MO, USA), subjected to three rounds of sonication and centrifuged at 13,400 g for 10 min. All procedures were carried out at 4 °C. Proteins were measured by the Bradford method using bovine serum albumin as standard.

5.11.2. Enzymatic assay

Hexosaminidase activity was determined using 3 mM 4-methy-lumbelliferyl-*N*-acetyl-β-d-glucosaminide (MUG) and 3 mM 4-methy-lumbelliferone-6-sulfo-2-acetamido-2-deoxy-β-d-glucopyranoside (MUGS) substrates dissolved in 0.1 M citrate/0.2 M disodium phosphate buffer at pH 4.5. The enzymatic reactions were performed using 50 µl of test sample incubated with 100 µl of substrate at 37 °C. All reactions were stopped by adding 2.850 ml of 0.2 M Glycine/NaOH, pH = 10.6. Fluorescence of the liberated 4-methylumbelliferone was measured on a Perkin Elmer LS3 spectro-fluorimeter (λ excitation 360 nm, λ emission 446 nm).

5.11.3. β-Hexosaminidase isoenzyme composition

Cell extracts were analysed by ion-exchange chromatography on Diethylaminoethyl- (DEAE)-Cellulose. Chromatography was performed using 0.5 ml column equilibrated with 10 mM sodium phosphate buffer, pH 6.0 (buffer A). The flow rate was 0.5 ml/min. Enzyme activity retained by the column was eluted by a linear gradient of NaCl (0.0–0.5 M in 20 ml of buffer B starting from fraction no. 20). Finally, the column was eluted with 1.0 M NaCl in buffer A. Fractions (0.5 ml) were collected and assayed for the Hex activity.

5.12. Cross-correction of SD NPCs and progeny

Donor cells (WT UT or LV.mAB-transduced SD NPCs) were plated on an adhesive substrate (matrigel) in medium containing FGF2 (20,000 cell/cm^2) (d0). After 48 h (d2), the supernatant (Sup) was removed and substituted with fresh medium without mitogens containing 2% FBS. This medium change was repeated at d4 and d6. The Sup collected at d4 and d6 was centrifuged to remove debris and used to treat *acceptor cells*

(SD UT) that had been plated under the same differentiating conditions. After a 24 h-washout with fresh medium, we collected acceptor cells and their Sup. Enzymatic activity was measured in the Sup and pellet of donor and acceptor cells, as described above.

5.13. Sphingolipid analysis

SD NPCs were plated on an adhesive substrate (matrigel) in medium containing FGF2 (20,000 cell/cm^2) supplemented with 12 nM of $[1-{}^3H]$-sphingosine (specific radioactivity 1.06 Ci/ mmol). After 48 h we removed the medium and incubated cells with either fresh medium or with the Supernatant (SUP) collected from donor cells, according to the cross-correction protocol described above. At the end of the experiment, cell lipids were extracted using the solvent system chloroform:methanol:water, 2:1:0.1, by volume. Total lipids extracts were subjected to phase separation according to Folch method with some modifications, as previously described (Samarani et al., 2018; Valsecchi et al., 2010). Finally, organic phases were subjected to alkaline methanolysis to remove glycerophospholipids (Valsecchi et al., 2010). Lipids contained in the organic and aqueous phases were separate by HPTLC using the solvent system chloroform:methanol:water 110:40:6 (v:v:v) and chloroform:methanol:CaCl$_2$ 0.2%, 50: 42:11 (v: v: v), respectively. Radioactive lipids were detected by digital autoradiography performed with a Beta-Imager ^{T}Racer system (BioSpace lab) and quantified using M3 vision software. Identification of lipids after separation was assessed by co-migration with authentic radioactive lipid standards.

5.14. Western blotting

Protein samples were extracted as described above. After boiling for 5 min in loading buffer, samples containing 40 μg protein were separated through a 4–12% gel SDS-PAGE electrophoresis. Western blotting was performed as previously described (Martino et al., 1995). Primary antibodies: monoclonal anti-α-subunit and polyclonal anti-β-subunit of Hex (anti-HexA, 1:1000, LS-C197404, LSBio; anti-HexB, 1:1000, LS-C354001, LSBio); rabbit anti calnexin, 1:5000, Sigma C4731. Immunodetection was performed using the Amersham ECL PlusTM kit (GE Healthcare).

5.15. Statistics

Data were analysed with Graph Pad Prism version 8.0 for Macintosh and expressed as the mean ± std. error of the mean (SEM). Unpaired Student t-test and One-way or Two-Way ANOVA followed by post-tests were used when appropriate (statistical significance: $P < .05$). The number of samples and the statistical test used are indicated in the legends of each figure.

Declaration of Competing Interest

The authors declare no conflicts of interest.

Acknowledgments

Appendix A. Supplementary data

Supplementary data to this article can be found online at https://doi.org/10.1016/j.nbd.2019.104667.

References

Aiuti, A., Biasco, L., Scaramuzza, S., Ferrua, F., Cicalese, M.P., Baricordi, C., Dionisio, F., Calabria, A., Giannelli, S., Castiello, M.C., Bosticardo, M., Evangelio, C., Assanelli, A., Casiraghi, M., Di Nunzio, S., Callegaro, L., Benati, C., Rizzardi, P., Pellin, D., Di Serio, C., Schmidt, M., Von Kalle, C., Gardner, J., Mehta, N., Neduva, V., Dow, D.J., Galy, A., Miniero, R., Finocchi, A., Metin, A., Banerjee, P.P., Orange, J.S., Galimberti, S., Valsecchi, M.G., Biffi, A., Montini, E., Villa, A., Ciceri, F., Roncarolo, M.G., Naldini, L., Aiuti, A., Biasco, L., Scaramuzza, S., Ferrua, F., Cicalese, M.P., Baricordi, C., Dionisio, F., Calabria, A., Giannelli, S., Carmina, M., et al., 2013. Lentiviral hematopoietic stem cell gene therapy in patients with Wiskott-Aldrich syndrome. Science (80-) 341, 1233151.

Amendola, M., Venneri, M.A., Biffi, A., Vigna, E., Naldini, L., 2005. Coordinate dual-gene transgenesis by lentiviral vectors carrying synthetic bidirectional promoters. Nat. Biotechnol. 23, 108–116.

Andersson, U., Smith, D., Jeyakumar, M., Butters, T.D., Borja, M.C., Dwek, R.A., Platt, F.M., 2004. Improved outcome of N-butyldeoxygalactonojirimycin-mediated substrate reduction therapy in a mouse model of Sandhoff disease. Neurobiol. Dis. 16, 506–515.

Arfi, A., Bourgoin, C., Basso, L., Emiliani, C., Tancini, B., Chigorno, V., Li, Y.T., Orlacchio, A., Poenaru, L., Sonnino, S., Caillaud, C., 2005. Bicistronic lentiviral vector corrects beta-hexosaminidase deficiency in transduced and cross-corrected human Sandhoff fibroblasts. Neurobiol. Dis. 20, 583–593.

Arfi, A., Zisling, R., Richard, E., Batista, L., Poenaru, L., Futerman, A.H., Caillaud, C., 2006. Reversion of the biochemical defects in murine embryonic Sandhoff neurons using a bicistronic lentiviral vector encoding hexosaminidase alpha and beta. J. Neurochem. 96, 1572–1579.

Ballabio, A., Gieselmann, V., 2009. Lysosomal disorders: from storage to cellular damage. Biochim. Biophys. Acta 1793, 684–696.

Bartholomae, C.C., Arens, A., Balaggan, K.S., Yanez-Munoz, R.J., Montini, E., Howe, S.J., Paruzynski, A., Korn, B., Appelt, J.U., Macneil, A., Cesana, D., Abel, U., Glimm, H., Naldini, L., Ali, R.R., Thrasher, A.J., von Kalle, C., Schmidt, M., 2011. Lentiviral vector integration profiles differ in rodent postmitotic tissues. Mol. Ther. 19, 703–710.

Biffi, A., Montini, E., Lorioli, L., Cesani, M., Fumagalli, F., Plati, T., Baldoli, C., Martino, S., Calabria, A., Canale, S., Benedicenti, F., Vallanti, G., Biasco, L., Leo, S., Kabbara, N., Zanetti, G., Rizzo, W.B., Mehta, N.A., Cicalese, M.P., Casiraghi, M., Boelens, J.J., Del Carro, U., Dow, D.J., Schmidt, M., Assanelli, A., Neduva, V., Di Serio, C., Stupka, E., Gardner, J., von Kalle, C., Bordignon, C., Ciceri, F., Rovelli, A., Roncarolo, M.G., Aiuti, A., Sessa, M., Naldini, L., 2013. Lentiviral hematopoietic stem cell gene therapy benefits metachromatic leukodystrophy. Science (80-) 341, 1233158.

Boitano, A.E., 2011. Aryl hydrocarbon receptor antagonists promote the expansion of human hematopoietic stem cells (science (2010) (1345)). Science 329 (5997), 1345–1348.

Bradbury, A.M., Cochran, J.N., McCurdy, V.J., Johnson, A.K., Brunson, B.L., Gray-Edwards, H., Leroy, S.G., Hwang, M., Randle, A.N., Jackson, L.S., Morrison, N.E., Baek, R.C., Seyfried, T.N., Cheng, S.H., Cox, N.R., Baker, H.J., Cachón-González, M.B., Cox, T.M., Sena-Esteves, M., Martin, D.R., Cachon-Gonzalez, M.B., Cox, T.M., Sena-Esteves, M., Martin, D.R., 2013. Therapeutic response in feline sandhoff disease despite immunity to intracranial gene therapy. Mol. Ther. 21, 1306–1315.

Cachon-Gonzalez, M.B., Wang, S.Z., Ziegler, R., Cheng, S.H., Cox, T.M., 2014. Reversibility of neuropathology in Tay-Sachs-related diseases. Hum. Mol. Genet. 23, 730–748.

Cantore, A., Ranzani, M., CC Bartholomae, M.V., Valle, P.D., Sanvito, F., LS Sergi, P., Gallina, F., Benedicenti, D., Bellinger, R., Raymer, E., Merricks, F., Bellintani, S., Martin, C., Doglioni, D'Angelo, A., Vanden Driessche, T., Chuah, M.K., Schmidt, M., Nichols, T., Montini, E., Naldini, L., 2015. Liver-directed lentiviral gene therapy in a dog model of hemophilia B. Sci. Transl. Med. 7, 277ra28.

Chiriaco, M., Farinelli, G., Capo, V., Zonari, E., Scaramuzza, S., Di Matteo, G., Sergi, L.S., Migliavacca, M., Hernandez, R.J., Bombelli, F., Giorda, E., Kajaste-Rudnitski, A., Trono, D., Grez, M., Rossi, P., Finocchi, A., Naldini, L., Gentner, B., Aiuti, A., 2014. Dual-regulated lentiviral vector for gene therapy of X-linked chronic granulomatosis. Mol. Ther. 22, 1472–1483.

Clarke, J.T.R., Mahuran, D.J., Sathe, S., Kolodny, E.H., Rigat, B.A., Raiman, J.A., Tropak, M.B., 2011. An open-label phase I/II clinical trial of pyrimethamine for the treatment of patients affected with chronic GM2 gangliosidosis (Tay-Sachs or Sandhoff variants). Mol. Genet. Metab. 102, 6–12.

Cutler, C., Multani, P., Robbins, D., Kim, H.T., Le, T., Hoggatt, J., Pelus, L.M., Desponts,

C., Bin Chen, Y., Rezner, B., Armand, P., Koreth, J., Glotzbecker, B., Ho, V.T., Alyea, E., Isom, M., Kao, G., Armant, M., L Silberstein, P.H., Soiffer, R.J., Scadden, D.T., Ritz, J., Goessling, W., North, T.E., Mendlein, J., Ballen, K., Zon, L.I., Antin, J.H., Shoemaker, D.D., 2013. Prostaglandin-modulated umbilical cord blood hematopoietic stem cell transplantation. Blood. 122 (17), 3074–3081.

Ellis, R.B., Ikonne, J.U., Masson, P.K., 1975. DEAE-cellulose microcolumn chromatography coupled with automated assay: application to the resolution of N-acetyl-β-d-hexosaminidase components. Anal. Biochem. 63 (1), 5–11.

Fares, I., Chagraoui, J., Lehnertz, B., MacRae, T., Mayotte, N., Tomellini, E., Aubert, L., Roux, P.P., Sauvageau, G., 2017. EPCR expression marks UM171-expanded CD34 + cord blood stem cells. Blood. 129 (25), 3334–3351.

Ferrua, F., Cicalese, M.P., Galimberti, S., Giannelli, S., Dionisio, F., Barzaghi, F., Migliavacca, M., Bernardo, M.E., Calbi, V., Assanelli, A.A., Facchini, M., Fossati, C., Albertazzi, E., Scaramuzza, S., Brigida, I., Scala, S., Basso-Ricci, L., Pajno, R., Casiraghi, M., Canarutto, D., Salerio, F.A., Albert, M.H., Bartoli, A., Wolf, H.M., Fiori, R., Silvani, P., Gattillo, S., Villa, A., Biasco, L., Dott, C., Culme-Seymour, E.J., van Rossem, K., Atkinson, G., Valsecchi, M.G., Roncarolo, M.G., Ciceri, F., Naldini, L., Aiuti, A., 2019. Lentiviral haemopoietic stem/progenitor cell gene therapy for treatment of Wiskott-Aldrich syndrome: interim results of a non-randomised, open-label, phase 1/2 clinical study. Lancet Haematol. 6 (5), e239–e253.

Frati, G., Luciani, M., Meneghini, V., De Cicco, S., Ståhlman, M., Blomqvist, M., Grossi, S., Filocamo, M., Morena, F., Menegon, A., Martino, S., Gritti, A., 2018. Human iPSC-based models highlight defective glial and neuronal differentiation from neural progenitor cells in metachromatic leukodystrophy. Cell Death Dis. 9, 698.

Gleitz, H.F.E., Liao, A.Y., Cook, J.R., Rowlston, S.F., Forte, G.M.A., Souza, Leary, Holley, R.J., Bigger, B.W., 2018. Brain-targeted stem cell gene therapy corrects mucopolysaccharidosis type II via multiple mechanisms. EMBO Mol. Med. 10 (7) (pii: e8730).

Golebiowski, D., van der Bom, I.M.J., Kwon, C.-S., Miller, A.D., Petrosky, K., Bradbury, A.M., Maitland, S., Kühn, A.L., Bishop, N., Curran, E., Silva, N., GuhaSarkar, D., Westmoreland, S.V., Martin, D.R., Gounis, M.J., Asaad, W.F., Sena-Esteves, M., 2017. Direct intracranial injection of AAVrh8 encoding monkey β-N-acetylhexosaminidase causes neurotoxicity in the primate brain. Hum. Gene Ther. 28, 510–522.

Gravel, R.A., Triggs-Raine, B.L., Mahuran, D.J., 1991. Biochemistry and genetics of Tay-Sachs disease. Can. J. Neurol. Sci. 18, 419–423.

Gray-Edwards, H.L., Randle, A.N., Maitland, S.A., Benatti, H.R., Hubbard, S.M., Canning, P.F., Vogel, M.B., Brunson, B.L., Hwang, M., Ellis, L.E., Bradbury, A.M., Gentry, A.S., Taylor, A.R., Wooldridge, A.A., Wilhite, D.R., Winter, R.L., Whitlock, B.K., Johnson, J.A., Holland, M., Salibi, N., Beyers, R.J., Sartin, J.L., Denney, T.S., Cox, N.R., Sena-Esteves, M., Martin, D.R., 2017. Adeno-associated virus gene therapy in a sheep model of Tay–Sachs disease. Hum. Gene Ther. 29 (3), 312–326.

Grieger, J.C., Samulski, R.J., 2012. Adeno-associated virus vectorology, manufacturing, and clinical applications. Methods Enzymol. 507, 229–254.

Gritti, A., Molin, M.D., Foroni, C., Bonfanti, L., Dal Molin, M., Foroni, C., Bonfanti, L., 2009. Effects of developmental age, brain region, and time in culture on long-term proliferation and multipotency of neural stem cell populations. J. Comp. Neurol. 517, 333–349.

Heffner, G.C., Bonner, M., Christiansen, L., Pierciey, F.J., Campbell, D., Smurnyy, Y., Zhang, W., Hamel, A., Shaw, S., Lewis, G., Goss, K.A., Garijo, O., Torbett, B.E., Horton, H., Finer, M.H., Gregory, P.D., Veres, G., 2018. Prostaglandin E 2 increases lentiviral vector transduction efficiency of adult human hematopoietic stem and progenitor cells. Mol. Ther. 26 (1), 320–328.

Hoogerbrugge, P.M., OF Brouwer, Bordigoni, P., Ringden, O., Kapaun, P., JJ Ortega, A.O., Meara, G., Cornu, G., Souillet, D., Frappaz, et al., 1995. Allogeneic bone marrow transplantation for lysosomal storage diseases. The European Group for Bone Marrow Transplantation. Lancet 345, 1398–1402.

Huang, J.Q., Trasler, J.M., Igdoura, S., Michaud, J., Hanai, N., Gravel, R.A., 1997. Apoptotic cell death in mouse models of G(M2) gangliosidosis and observations on human Tay-Sachs and Sandhoff diseases. Hum. Mol. Genet. 6, 1879–1885.

Ikonne, J.U., Rattazzi, M.C., Desnick, R.J., 1975. Characterization of hex S, the major residual beta hexosaminidase activity in type O Gm2 gangliosidosis (Sandhoff-Jatzkewitz disease). Am. J. Hum. Genet. 27 (5), 639–650.

Klein, D., Yaghootfam, A., Matzner, U., Koch, B., Braulke, T., Gieselmann, V., 2009. Mannose 6-phosphate receptor-dependent endocytosis of lysosomal enzymes is increased in sulfatide-storing kidney cells. Biol. Chem. 390, 41–48.

Lattanzi, A., Neri, M., Maderna, C., di Girolamo, I., Martino, S., Orlacchio, A., Amendola, M., Naldini, L., Gritti, A., 2010. Widespread enzymatic correction of CNS tissues by a single intracerebral injection of therapeutic lentiviral vector in leukodystrophy mouse models. Hum. Mol. Genet. 19, 2208–2227.

Lattanzi, A., Salvagno, C., Maderna, C., Benedicenti, F., Morena, F., Kulik, W., Naldini, L., Montini, E., Martino, S., Gritti, A., 2014. Therapeutic benefit of lentiviral-mediated neonatal intracerebral gene therapy in a mouse model of globoid cell leukodystrophy. Hum. Mol. Genet. 23, 3250–3268.

Maegawa, G.H.B., Tropak, M., Buttner, J., Stockley, T., Kok, F., Clarke, J.T.R., Mahuran, D.J., 2007. Pyrimethamine as a potential pharmacological chaperone for late-onset forms of GM2 gangliosidosis. J. Biol. Chem. 282, 9150–9161.

Maegawa, G.H.B., Banwell, B.L., Blaser, S., Sorge, G., Toplak, M., Ackerley, C., Hawkins, C., Hayes, J., Clarke, J.T.R., 2009. Substrate reduction therapy in juvenile GM2 gangliosidosis. Mol. Genet. Metab. 98, 215–224.

Markmann, S., Thelen, M., Cornils, K., Schweizer, M., Brocke-Ahmadinejad, N., Willnow, T., Heeren, J., Gieselmann, V., Braulke, T., Kollmann, K., 2015. Lrp1/LDL receptor play critical roles in mannose 6-phosphate-independent lysosomal enzyme targeting. Traffic 16 (7), 743–759.

Marktel, S., Scaramuzza, S., Cicalese, M.P., Giglio, F., Galimberti, S., Lidonnici, M.R., Calbi, V., Assanelli, A., Bernardo, M.E., Rossi, C., Calabria, A., Milani, R., Gattillo, S., Benedicenti, F., Spinozzi, G., Aprile, A., Bergami, A., Casiraghi, M., Consiglieri, G., Masera, N., D'Angelo, E., Mirra, N., Origa, R., Tartaglione, I., Perrotta, S., Winter, R.,

Coppola, M., Viarengo, G., Santoleri, L., Graziadei, G., Gabaldo, M., Valsecchi, M.G., Montini, E., Naldini, L., Cappellini, M.D., Ciceri, F., Aiuti, A., Ferrari, G., 2019. Intrabone hematopoietic stem cell gene therapy for adult and pediatric patients affected by transfusion-dependent ß-thalassemia. Nat. Med. 25, 234–241.

Martino, S., Emiliani, C., Orlacchio, A., Hosseini, R., Stirling, J.L., 1995. Beta-N-acetylhexosaminidases A and S have similar sub-cellular distributions in HL-60 cells. Biochim. Biophys. Acta 1243, 489–495.

Martino, S., Emiliani, C., Tabilio, A., Falzetti, F., Stirling, J.L., Orlacchio, A., 1997. Distribution of active alpha- and beta-subunits of beta-N-acetylhexosaminidase as a function of leukaemic cell types. Biochim. Biophys. Acta 1335, 5–15.

Martino, S., Emiliani, C., Tancini, B., Severini, G.M., Chigorno, V., Bordignon, C., Sonnino, S., Orlacchio, A., 2002. Absence of metabolic cross-correction in Tay-Sachs cells: implications for gene therapy. J. Biol. Chem. 277, 20177–20184.

Martino, S., Marconi, P., Tancini, B., Dolcetta, D., De Angelis, M.G., Montanucci, P., Bregola, G., Sandhoff, K., Bordignon, C., Emiliani, C., Manservigi, R., Orlacchio, A., 2005. A direct gene transfer strategy via brain internal capsule reverses the biochemical defect in Tay-Sachs disease. Hum. Mol. Genet. 14, 2113–2123.

Martino, S., Di Girolamo, I., Cavazzin, C., Tiribuzi, R., Galli, R., Rivaroli, A., Valsecchi, M., Sandhoff, K., Sonnino, S., Vescovi, A., Gritti, A., Orlacchio, A., 2009. Neural precursor cell cultures from GM2 gangliosidosis animal models recapitulate the biochemical and molecular hallmarks of the brain pathology. J. Neurochem. 109, 135–147.

Matsuoka, K., Tamura, T., Tsuji, D., Dohzono, Y., Kitakaze, K., Ohno, K., Saito, S., Sakuraba, H., Itoh, K., 2011. Therapeutic potential of intracerebroventricular replacement of modified human β-hexosaminidase B for GM2 gangliosidosis. Mol. Ther. 19, 1017–1024.

McCurdy, V.J., Rockwell, H.E., Arthur, J.R., Bradbury, A.M., Johnson, A.K., Randle, A.N., Brunson, B.L., Hwang, M., Gray-Edwards, H.L., Morrison, N.E., Johnson, J.A., Baker, H.J., Cox, N.R., Seyfried, T.N., Sena-Esteves, M., Martin, D.R., 2015. Widespread correction of central nervous system disease after intracranial gene therapy in a feline model of Sandhoff disease. Gene Ther. 22, 181–189.

Meneghini, V., Lattanzi, A., Tiradani, L., Bravo, G., Morena, F., Sanvito, F., Calabria, A., Bringas, J., Fisher-Perkins, J.M., Dufour, J.P., Baker, K.C., Doglioni, C., Montini, E., Bunnell, B.A., Bankiewicz, K., Martino, S., Naldini, L., Gritti, A., 2016. Pervasive supply of therapeutic lysosomal enzymes in the CNS of normal and Krabbe-affected non-human primates by intracerebral lentiviral gene therapy. EMBO Mol. Med. 8, 489–510.

Meneghini, V., Frati, G., Sala, D., De Cicco, S., Luciani, M., Cavazzin, C., Paulis, M., Mentzen, W., Morena, F., Giannelli, S., Sanvito, F., Villa, A., Bulfone, A., Broccoli, V., Martino, S., Gritti, A., 2017. Generation of human induced pluripotent stem cell-derived Bona fide neural stem cells for ex vivo gene therapy of metachromatic leukodystrophy. Stem Cells Transl. Med. 6, 352–368.

Mingozzi, F., High, K.A., 2013. Immune responses to AAV vectors: overcoming barriers to successful gene therapy. Blood 122, 23–36.

Neri, M., Ricca, A., Di Girolamo, I., Alcala'-Franco, B., Cavazzin, C., Orlacchio, A., Martino, S., Naldini, L., Gritti, A., Alcala, B., Franco, Cavazzin, C., Orlacchio, A., Martino, S., Naldini, L., Gritti, A., Alcala'-Franco, B., Cavazzin, C., Orlacchio, A., Martino, S., Naldini, L., Gritti, A., 2011. Neural stem cell gene therapy ameliorates pathology and function in a mouse model of globoid cell leukodystrophy. Stem Cells 29, 1559–1571.

Norflus, F., Tifft, C.J., McDonald, M.P., Goldstein, G., Crawley, J.N., Hoffmann, A., Sandhoff, K., Suzuki, K., Proia, R.L., 1998. Bone marrow transplantation prolongs life span and ameliorates neurologic manifestations in Sandhoff disease mice. J. Clin. Invest. 101, 1881–1888.

Ohsawa, M., Kotani, M., Tajima, Y., Tsuji, D., Ishibashi, Y., Kuroki, A., Itoh, K., Watabe, K., Sango, K., Yamanaka, S., Sakuraba, H., 2005. Establishment of immortalized Schwann cells from Sandhoff mice and corrective effect of recombinant human b-hexosaminidase a on the accumulated GM2 ganglioside. J. Hum. Genet. 50, 460–467.

Osmon, K.J.L., Woodley, E., Thompson, P., Ong, K., Karumuthil-Melethil, S., Keimel, J.G., Mark, B.L., Mahuran, D., Gray, S.J., Walia, J.S., 2016. Systemic gene transfer of a hexosaminidase variant using an scAAV9.47 vector corrects GM2 gangliosidosis in Sandhoff mice. Hum. Gene Ther. 27, 497–508.

Oya, Y., Proia, R.L., Norflus, F., Tifft, C.J., Langaman, C., Suzuki, K., 2000. Distribution of enzyme-bearing cells in GM2 gangliosidosis mice: regionally specific pattern of cellular infiltration following bone marrow transplantation. Acta Neuropathol. 99, 161–168.

Palfi, S., Gurruchaga, J.M., Ralph, G.S., Lepetit, H., Lavisse, S., Buttery, P.C., Watts, C., Miskin, J., Kelleher, M., Deeley, S., Iwamuro, H., Lefaucheur, J.P., Thiriez, C., Fenelon, G., Lucas, C., Brugieres, P., Gabriel, I., Abhay, K., Drouot, X., Tani, N., Kas, A., Ghaleh, B., Le Corvoisier, P., Dolphin, P., Breen, D.P., Mason, S., Guzman, N.V., Mazarakis, N.D., Radcliffe, P.A., Harrop, R., Kingsman, S.M., Rascol, O., Naylor, S., Barker, R.A., Hantraye, P., Remy, P., Cesaro, P., Mitrophanous, K.A., 2014. Long-term safety and tolerability of ProSavin, a lentiviral vector-based gene therapy for Parkinson's disease: a dose escalation, open-label, phase 1/2 trial. Lancet 383, 1138–1146.

Petrillo, C., Cesana, D., Piras, F., Bartolaccini, S., Naldini, L., Montini, E., Kajaste-Rudnitski, A., 2015. Cyclosporin a and rapamycin relieve distinct lentiviral restriction blocks in hematopoietic stem and progenitor cells. Mol. Ther. 23 (2), 352–362.

Petrillo, C., Thorne, L.G., Unali, G., Schiroli, G., Giordano, A.M.S., Piras, F., Cuccovillo, I., Petit, S.J., Ahsan, F., Noursadeghi, M., Clare, S., Genovese, P., Gentner, B., Naldini, L., Towers, G.J., Kajaste-Rudnitski, A., 2018. Cyclosporine H overcomes innate immune restrictions to improve lentiviral transduction and gene editing in human hematopoietic stem cells. Cell Stem Cell 23 (6), 820–832.

Phaneuf, D., Wakamatsu, N., Huang, J.Q., Borowski, A., Peterson, A.C., Fortunato, S.R., Ritter, G., Igdoura, S.A., Morales, C.R., Benoit, G., Akerman, B.R., Leclerc, D., Hanai, N., Marth, J.D., Trasler, J.M., Gravel, R.A., 1996. Dramatically different phenotypes in mouse models of human Tay-Sachs and Sandhoff diseases. Hum. Mol. Genet. 5,

1–14.

Regier, D.S., Proia, R.L., D'Azzo, A., Tifft, C.J., 2016. The GM1 and GM2 Gangliosidoses: natural history and Progress toward therapy. Pediatr. Endocrinol. Rev. 13, 663–673.

Ricca, A., Rufo, N., Ungari, S., Morena, F., Martino, S., Kulik, W., Alberizzi, V., Bolino, A., Bianchi, F., Del Carro, U., Biffi, A., Gritti, A., 2015. Combined gene/cell therapies provide long-term and pervasive rescue of multiple pathological symptoms in a murine model of globoid cell leukodystrophy. Hum. Mol. Genet. 24 (12), 3372–3389.

Rockwell, H.E., McCurdy, V.J., Eaton, S.C., Wilson, D.U., Johnson, A.K., Randle, A.N., Bradbury, A.M., Gray-Edwards, H.L., Baker, H.J., Hudson, J.A., Cox, N.R., Sena-Esteves, M., Seyfried, T.N., Martin, D.R., 2015. AAV-mediated gene delivery in a feline model of Sandhoff disease corrects lysosomal storage in the central nervous system. ASN Neuro 7 (2) (pii: 1759091415569908).

Samarani, M., Loberto, N., Soldà, G., Straniero, L., Asselta, R., Duga, S., Lunghi, G., FA Zucca, L.M., Ciampa, M.G., Schiumarini, D., Bassi, R., Giussani, P., Chiricozzi, E., Prinetti, A., Aureli, M., Sonnino, S., 2018. A lysosome–plasma membrane—sphingolipid axis linking lysosomal storage to cell growth arrest. FASEB J. 32 (10), 5685–5702.

Sandhoff, K., Harzer, K., 2013. Gangliosides and gangliosidoses: principles of molecular and metabolic pathogenesis. J. Neurosci. 33, 10195–10208.

Sango, K., McDonald, M.P., Crawley, J.N., Mack, M.L., Tifft, C.J., Skop, E., Starr, C.M., Hoffmann, A., Sandhoff, K., Suzuki, K., Proia, R.L., 1996. Mice lacking both subunits of lysosomal beta-hexosaminidase display gangliosidosis and mucopolysaccharidosis. Nat. Genet. 14, 348–352.

Sango, K., Yamanaka, S., Ajiki, K., Tokashiki, A., Watabe, K., 2002. Lysosomal storage results in impaired survival but normal neurite outgrowth in dorsal root ganglion neurones from a mouse model of Sandhoff disease. Neuropathol. Appl. Neurobiol. 28, 23–34.

Santoni de Sio, F.R., Cascio, P., Zingale, A., Gasparini, M., Naldini, L., 2006. Proteasome activity restricts lentiviral gene transfer into hematopoietic stem cells and is down-regulated by cytokines that enhance transduction. Blood 107, 4257–4265.

Scaramuzza, S., Biasco, L., Ripamonti, A., MC Castiello, M., Loperfido, E.D., Hernandez, R.J., Benedicenti, F., Radrizzani, M., Salomoni, M., Ranzani, M., Bartholomae, C.C., Vicenzi, E., Finocchi, A., Bredius, R., Bosticardo, M., von Schmidt, M., Kalle, C., Montini, E., Biffi, A., Roncarolo, M.G., Naldini, L., Villa, A., Aiuti, A., 2013. Preclinical safety and efficacy of human CD34(+) cells transduced with lentiviral vector for the treatment of Wiskott-Aldrich syndrome. Mol. Ther. 21, 175–184.

Sessa, M., Lorioli, L., Fumagalli, F., Acquati, S., Redaelli, D., Baldoli, C., Canale, S., Lopez, I.D., Morena, F., Calabria, A., Fiori, R., Silvani, P., Rancoita, P.M.V., Gabaldo, M., Benedicenti, F., Antonioli, G., Assanelli, A., Cicalese, M.P., del Carro, U., Sora, M.G.N., Martino, S., Quattrini, A., Montini, E., Di Serio, C., Ciceri, F., Roncarolo, M.G., Aiuti, A., Naldini, L., Biffi, A., 2016. Lentiviral haemopoietic stem-cell gene therapy in early-onset metachromatic leukodystrophy: an ad-hoc analysis of a non-randomised, open-label, phase 1/2 trial. Lancet 388, 476–487.

Sinici, I., Yonekawa, S., Tkachyova, I., Gray, S.J., Samulski, R.J., Wakarchuk, W., Mark, B.L., Mahuran, D.J., 2013. In cellulo examination of a Beta-alpha hybrid construct of beta-hexosaminidase a subunits, reported to interact with the GM2 activator protein and hydrolyze GM2 ganglioside. PLoS One 8 (3), e57908.

Sorrentino, N.C., D'Orsi, L., Sambri, I., Nusco, E., Monaco, C., Spampanato, C., Polishchuk, E., Saccone, P., De Leonibus, E., Ballabio, A., Fraldi, A., 2013. A highly secreted sulphamidase engineered to cross the blood-brain barrier corrects brain lesions of mice with mucopolysaccharidoses type IIIA. EMBO Mol. Med. 5, 675–690.

Szymczak-Workman, A.L., Vignali, K.M., Vignali, D.A.A., 2012. Design and construction of 2A peptide-linked multicistronic vectors. Cold Spring Harb Protoc (2), 199–204 2012.

Tallaksen, C.M.E., Berg, J.E., 2009. Miglustat therapy in juvenile Sandhoff disease. J.

Inherit. Metab. Dis. 32.

Tropak, M.B., Yonekawa, S., Karumuthil-Melethil, S., Thompson, P., Wakarchuk, W., Gray, S.J., Walia, J.S., Mark, B.L., Mahuran, D., 2016. Construction of a hybrid β-hexosaminidase subunit capable of forming stable homodimers that hydrolyze GM2 ganglioside in vivo. Mol. Ther. Meth. Clin. Dev. 3, 15057.

Tsuji, D., Kuroki, A., Ishibashi, Y., Itakura, T., Itoh, K., 2005. Metabolic correction in microglia derived from Sandhoff disease model mice. J. Neurochem. 94, 1631–1638.

Tsuji, D., Akeboshi, H., Matsuoka, K., Yasuoka, H., Miyasaki, E., Kasahara, Y., Kawashima, I., Chiba, Y., Jigami, Y., Taki, T., Sakuraba, H., Itoh, K., 2011. Highly phosphomannosylated enzyme replacement therapy for GM2 gangliosidosis. Ann. Neurol. 69, 691–701.

Ungari, S., Montepeloso, A., Morena, F., Cocchiarella, F., Recchia, A., Martino, S., Gentner, B., Naldini, L., Biffi, A., 2015. Design of a regulated lentiviral vector for hematopoietic stem cell gene therapy of globoid cell leukodystrophy. Mol. Ther. Meth. Clin. Dev. 2, 15038.

Utsumi, K., Tsuji, A., Kase, R., Tanaka, A., Tanaka, T., Uyama, E., Ozawa, T., Sakuraba, H., Komaba, Y., Kawabe, M., Iino, Y., Katayama, Y., 2002. Western blotting analysis of the beta-hexosaminidase alpha- and beta-subunits in cultured fibroblasts from cases of various forms of GM2 gangliosidosis. Acta Neurol. Scand. 105, 427–430.

Valsecchi, M., Aureli, M., Mauri, L., Illuzzi, G., Chigorno, V., Prinetti, A., Sonnino, S., 2010. Sphingolipidomics of A2780 human ovarian carcinoma cells treated with synthetic retinoids. J. Lipid Res. 51 (7), 1832–1840.

Vigna, E., Amendola, M., Benedicenti, F., Simmons, A.D., Follenzi, A., Naldini, L., 2005. Efficient Tet-dependent expression of human factor IX in vivo by a new self-regulating lentiviral vector. Mol. Ther. 11, 763–775.

Visigalli, I., Delai, S., Politi, L.S., Di Domenico, C., Cerri, F., Mrak, E., D'Isa, R., Ungaro, D., Stok, M., Sanvito, F., Mariani, E., Staszewsky, L., Godi, C., Russo, I., Cecere, F., Del Carro, U., Rubinacci, A., Brambilla, R., Quattrini, A., Di Natale, P., Ponder, K., Naldini, L., Biffi, A., 2010. Gene therapy augments the efficacy of hematopoietic cell transplantation and fully corrects mucopolysaccharidosis type I phenotype in the mouse model. Blood 116, 5130–5139.

von Specht, B.U., Geiger, B., Arnon, R., Passwell, J., Keren, G., Goldman, B., Padeh, B., 1979. Enzyme replacement in Tay-Sachs disease. Neurology 29, 848–854.

Wada, R., Tifft, C.J., Proia, R.L., 2000. Microglial activation precedes acute neurodegeneration in Sandhoff disease and is suppressed by bone marrow transplantation. Proc. Natl. Acad. Sci. U. S. A. 97, 10954–10959.

Wagner, J.E., Brunstein, C.G., Boitano, A.E., Defor, T.E., McKenna, D., Sumstad, D., Blazar, B.R., Tolar, J., Le, C., Jones, J., Cooke, M.P., Bleul, C.C., 2016. Phase I/II trial of StemRegenin-1 expanded umbilical cord blood hematopoietic stem cells supports testing as a stand-alone graft. Cell Stem Cell 18 (1), 144–155.

Wang, C.X., Sather, B.D., Wang, X., Adair, J., Khan, I., Singh, S., Lang, S., Adams, A., Curinga, G., Kiem, H.P., Miao, C.H., Rawlings, D.J., Torbett, B.E., 2014. Rapamycin relieves lentiviral vector transduction resistance in human and mouse hematopoietic stem cells. Blood. 124 (6), 913–923.

Watts, K.L., Delaney, C., Nelson, V., Trobridge, G.D., Beard, B.C., Humphries, R.K., Kiem, H.P., 2013. CD34 + expansion with delta-1 and hoxb4 promotes rapid engraftment and transfusion independence in a macaca nemestrina cord blood transplant model. Mol. Ther. 21 (6), 1270–1278.

Woodley, E., Osmon, K.J.L., Thompson, P., Richmond, C., Chen, Z., Gray, S.J., Walia, J.S., 2019. Efficacy of a bicistronic vector for correction of Sandhoff disease in a mouse model. Mol. Ther. Meth. Clin. Dev. 12, 47–57.

Zonari, E., Desantis, G., Petrillo, C., Boccalatte, F.E., Lidonnici, M.R., Kajaste-Rudnitski, A., Aiuti, A., Ferrari, G., Naldini, L., Gentner, B., 2017. Efficient ex vivo engineering and expansion of highly purified human hematopoietic stem and progenitor cell populations for gene therapy. Stem Cell Rep. 8 (4), 977–990.